Available online at www.sciencedirect.com
ScienceDirect
Geochimica et Cosmochimica Acta 74 (2010) 144–163
Geochimica et Cosmochimica Acta
www.elsevier.com/locate/gca

The behavior of molybdenum and its isotopes across the chemocline and in the sediments of sulfidic Lake Cadagno, Switzerland

Tais W. Dahl [a,*], Ariel D. Anbar [b], Gwyneth W. Gordon [b], Minik T. Rosing [a], Robert Frei [c], Donald E. Canfield [d]

[a] *Nordic Center for Earth Evolution (NordCEE) and Geological Museum, University of Copenhagen, Øster Voldgade 5-7, DK-1350 Copenhagen K, Denmark*
[b] *School of Earth and Space Exploration, Department of Chemistry and Biochemistry, Arizona State University, Tempe, AZ 85287, USA*
[c] *Nordic Center for Earth Evolution (NordCEE) and Institute for Geography and Geology, University of Copenhagen, Øster Voldgade 10, DK-1350 Copenhagen K, Denmark*
[d] *Nordic Center for Earth Evolution (NordCEE) and Biological Institute, University of Southern Denmark, Campusvej 55, DK-5230 Odense M, Denmark*

Received 16 March 2009; accepted in revised form 15 September 2009; available online 22 September 2009

Abstract

Molybdenum (Mo) isotope studies in black shales can provide information about the redox evolution of the Earth's oceans, provided the isotopic consequences of Mo burial into its major sinks are well understood. Previous applications of the Mo isotope paleo-ocean redox proxy assumed quantitative scavenging of Mo when buried into sulfidic sediments. This paper contains the first complete suite of Mo isotope fractionation observations in a sulfidic water column and sediment system, the meromictic Lake Cadagno, Switzerland, a small alpine lake with a pronounced oxygen–sulfide transition reaching up to $H_2S \sim 200$ μM in the bottom waters (or about 300 μM total sulfide: $\Sigma S^{2-} = H_2S + HS^- + S^{2-}$). We find that Mo behaves conservatively in the oxic zone and non-conservatively in the sulfidic zone, where dissolved Mo concentrations decrease from 14 nM to 2–8 nM across this transition. Dissolved Mo in the upper oxic waters has a $\delta^{98}Mo_{oxic} = 0.9 \pm 0.1‰$, which matches that of the riverine input, $\delta^{98}Mo_{river} = 0.9 \pm 0.1‰$. In the deeper sulfidic waters, a subaquatic source delivers Mo at $1.55 \pm 0.1‰$, but the dissolved Mo is even heavier at $\delta^{98}Mo_{sulfidic} = 1.8‰$. Sediment traps in the sulfidic zone of the lake collect particles increasingly enriched in Mo with depth, with $\delta^{98}Mo$ values significantly fractionated at $-0.8‰$ to $-1.2‰$ both near the chemocline and in the deepest trap. Suspended particulates in the sulfidic waters carry lighter Mo than the ambient dissolved Mo pool by ~0.3–1.5‰. Sedimentary Mo concentrations correlate with total organic carbon and yield Mo levels which are two orders of magnitude higher than typical crustal values found in rocks from the catchment area. Solid-phase Mo in the sediment shows a slightly positive $\delta^{98}Mo$ trend with depth, from $\delta^{98}Mo = 1.2‰$ to $1.4‰$ while the pore waters show dramatic enrichments of Mo (>2000 nM) with a relatively light isotope signature of $\delta^{98}Mo = 0.9$–$1.0‰$.

These data are explained if Mo is converted to particle-reactive oxythiomolybdates in the sulfidic waters and is fractionated during removal from solution onto particles. Isotope fractionation is expressed in the water column, despite the high sulfide concentrations, because the rate of Mo removal is fast compared to the slow reaction kinetics of thiomolybdate formation. However, elemental and isotopic mass balances show that Mo is indeed quantitatively removed to the lake sediments and thus the isotopic composition of the sediments reflects sources to the sulfidic water. This efficient Mo drawdown is expected to occur in settings where H_2S is very much in excess over Mo or in a restricted setting where the water renewal rate is slow compared to the Mo burial rate. We present a model for the Mo isotope fractionation in sulfidic systems associated with

* Corresponding author. Present address: Department of Organismic and Evolutionary Biology, Harvard University, 26 Oxford St., Cambridge, MA 02138, USA. Tel.: +1 617 4957602; fax: +1 617 4955667.
E-mail address: tdahl@fas.harvard.edu (T.W. Dahl).

doi:10.1016/j.gca.2009.09.018

the slow reaction kinetics and conclude that quantitative removal will occur in highly sulfidic and restricted marine systems.

1. INTRODUCTION

The fractionation of molybdenum (Mo) isotopes in ancient sediments holds information on the evolution of global marine redox state (Arnold et al., 2004; Lehmann et al., 2007; Pearce et al., 2008; Wille et al., 2008; Gordon et al., 2009; Kendall et al., 2009). In the modern ocean, molybdate has a long residence time (~800 kyrs) and is well-mixed (Morford and Emerson, 1999; Siebert et al., 2003). Due to its long residence time, Mo is also the most abundant transition metal in the ocean at ~105 nM (Collier, 1985). Today's oceans display a heavy Mo isotope composition of $\delta^{98}Mo_{ocean} = 2.3 \pm 0.1‰$ relative to the average crust ($\delta^{98}Mo_{crust} \sim 0‰$; (Siebert et al., 2003; Nakagawa et al., 2008), and this has been attributed to the removal of isotopically light Mo of $\delta^{98}Mo = -0.7 \pm 0.1‰$ by adsorption onto Mn-oxyhydroxides (Siebert et al., 2003; Barling and Anbar, 2004). Another major Mo sink are sediments underlying a sulfidic (euxinic) water column, because Mo is readily scavenged under sulfidic conditions. The isotopic composition of these sediments is variably offset (Arnold et al., 2004; Neubert et al., 2008) with no offset during quantitative removal of Mo from the sulfidic water column where any isotope fractionation will not be expressed. This is what is observed in the Black Sea (Neubert et al., 2008) and is considered normal for sediments in euxinic water bodies. Because of the isotopic difference between the oxic and euxinic sinks, and because euxinic sediments seem to record seawater values, the isotopic composition of ancient euxinic shales may be used to understand the fraction of Mo removal into euxinic versus oxic environments and the extent of ancient sulfidic conditions in the ocean (Siebert et al., 2003; Arnold et al., 2004). For example, it has been proposed that the ocean contained substantial expanses of sulfidic water during much of the Proterozoic (Canfield, 1998) changing the balance of isotopic sinks and dictating the Mo isotopic composition of the Proterozoic ocean (Arnold et al., 2004; Kendall et al., 2009).

The pathway of Mo removal from oxygenated waters into sulfidic sediments involves a conversion of molybdate to particle-reactive thiomolybdates in the presence of >11 μM H_2S. We measure total sulfide with Cline reagent, which includes all dissolved protonated and non-protonated species: $\Sigma S^{2-} = H_2S + HS^- + S^{2-}$. As H_2S is the sulfide reactive form towards molybdate, its concentration must be calculated from the Cline total sulfide results, pH, and equilibrium constants for the different protonation reactions. Sulfidation of molybdate, however, is a slow process, and metastable oxythiomolybdates prevail in many natural sulfidic systems (Erickson and Helz, 2000). The pathways of particle-reactive Mo removal remain in dispute, but experiments have shown that Mo(VI) adsorbs both to pyrite and organic matter at neutral pH (Helz et al., 1996). On pyrite, tetrathiomolybdate MoS_4^{2-} adsorbs irreversibly while molybdate easily desorbs (Bostick et al., 2003). A higher particle affinity has also been observed for the more sulfidated species in adsorption experiments with FeS (Helz et al., 2004).

The isotope fractionation factor between species A and B is given in terms of $^{98}\alpha_{A-B} = (^{98}Mo/^{95}Mo)_A/(^{98}Mo/^{95}Mo)_B$ and we adopt the approximation $^{98}\Delta_{A-B} \approx 10^3(^{98}\alpha_{A-B}-1)$ to represent the isotope offset between product (A) and reactant (B). Theory predicts an equilibrium fractionation factor of $^{98}\Delta_{tetrathiomolybdate-molybdate} = -6.2‰$ at 4.8 °C with about a −1.5‰ shift for each sulfidation step, $MoO_{4-x}S_x^{2-}$, where $x = 0 \rightarrow 1 \rightarrow 2 \rightarrow 3 \rightarrow 4$. (Tossell, 2005). Each successive sulfidation step progresses 10 times slower than the previous one (Erickson and Helz, 2000), so the isotope fractionation associated with the first steps are likely not expressed in stagnant waters, where there is sufficient time for conversion to more sulfidated Mo. For example, where particles capture all tetrathiomolybdate and dissolved Mo remains as pure trithiomolybdate, one should find $^{98}\Delta_{part-diss} = {}^{98}\Delta_{tetrathio-trithio} = -1.7‰$ (interpolation from Tossell, 2005). For comparison, molybdate adsorbs onto Mn-oxides with an equilibrium fractionation ($^{98}\Delta_{sorbed-molybdate}$) of −2.8‰ (Barling and Anbar, 2004; Wasylenki et al., 2008).

In an effort to evaluate the robustness of the Mo isotopic paleo-ocean redox proxy, we aim to address five important questions about the removal pathways of Mo and their isotopic implications: (1) are Mo isotopes fractionated during removal at oxic-sulfidic boundaries?, (2) do diagenetic processes change the Mo isotopic composition?, (3) what controls Mo isotope fractionation in sulfidic water columns (adsorption, sulfidation, or reduction to Mo^{IV})?, (4) what is the nature of the particles to which Mo adsorbs under sulfidic conditions? and (5) do $\delta^{98}Mo$ values in euxinic sediments reflect the Mo isotopic composition of the overlying water column? Our study is based on measurements of Mo elemental and isotopic abundances in the water column, sediments, pore water, source materials, suspended particles, and sinking particles in the meromictic Lake Cadagno.

2. SITE DESCRIPTION

Lake Cadagno is a 21 m deep alpine meromictic (permanently stratified) lake situated at an altitude of 1921 m in Piora Valley in the southern part of central Switzerland (Fig. 1). The local bedrock includes felsic gneiss, dolomite and gypsum. The lake basin was created by glacial erosion and was dammed by a moraine during the last glaciation of the valley about 8000 yrs ago. The water body has three distinct layers, the oxic mixolimnion, a narrow chemocline at ~11 m depth in which anoxygenic phototrophic organisms thrive, and an anoxic and sulfidic monimolimnion. This structure is maintained by the density difference between dense solute-rich water constantly supplied by subaquatic springs to the monimolimnion and the low-salinity river

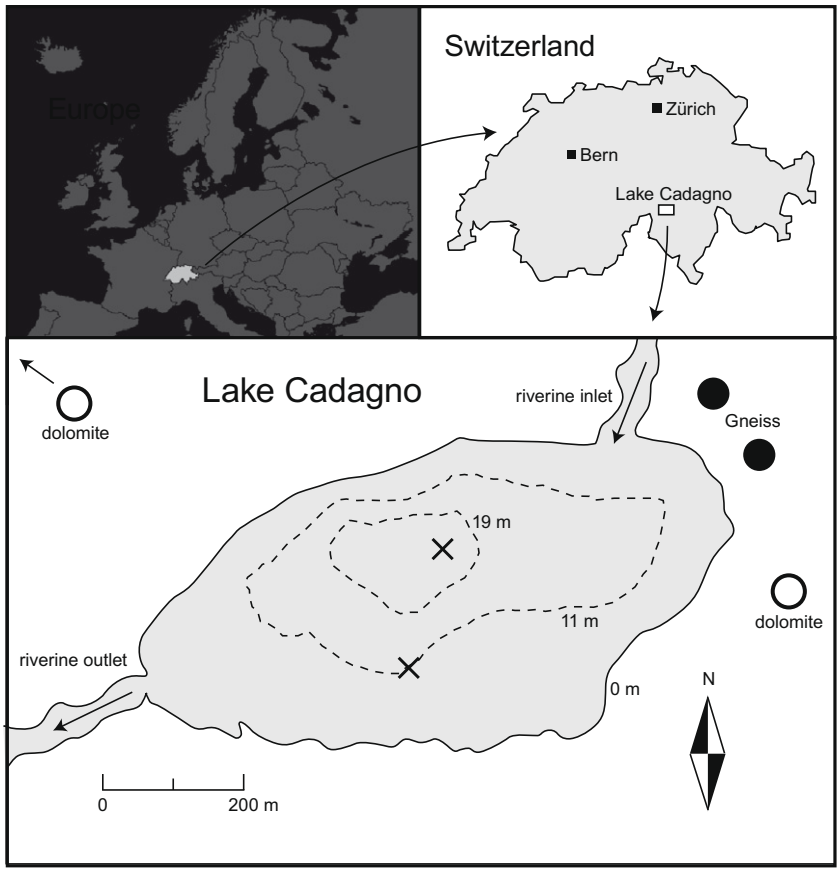

Fig. 1. Geographical map of Lake Cadagno, Switzerland. Water column studies have been performed within the >19 m depth zone. The approximate location of our samples are marked on the map: sediment cores are taken from the deepest point and 11 m depth (×), outcrop samples of gneisses (●) and dolomites (○) have been taken from the catchment area. The riverine inflow to the lake was sampled from a creek at a major waterfall on the northeast side of the lake. Water from swamps just 50 m west of the creek were sampled for comparison. The riverine outflow was sampled from a creek on the western part of the lake.

water supplying the mixolimnion (for example Uhde, 1992; Del Don et al., 2001). This redox stratification is known to have existed for more than 100 yrs (Del Don et al., 2001).

3. METHODS

3.1. Sampling

Samples were taken during field trips in June 2006, September 2006, and August 2007. Water was pumped using a metal-free *Flojet Quiet Quad* pump system and sampled for sulfide, sulfate, oxygen, pH, Sr isotopic compositions and Mo concentrations. We sampled water from ~20 depths from the surface to 20 m by pumping the water into a clean plastic bucket and this water was sub-sampled with a plastic syringe. Both bucket and a syringe were rinsed with the water from the respective depths, and the syringe was rinsed in water several times to avoid air bubbles or oxidation of the sample. For metal concentration determinations, we collected unfiltered water, filtered water and the particulates. Oxidation of the samples is limited by the short sampling time (less than 1 min) and the slow reaction kinetics of thiomolybdate to molybdate. We used *Advantec* glass fiber filters (GF-75 or GC-50 with pore size of ~0.7 μm and ~1.2 μm, respectively). The particulate was leached from the filters with 2N HNO_3. All acids used were singly distilled, if not otherwise stated. Dilutions are made in 18.2 MΩ milli-Q H_2O.

For Mo isotope analysis, water samples of 2–5 L were pumped from the lake through plastic tubing and stored in acid-cleaned polyethylene containers. Water samples were filtered at the Lake Cadagno field station using the same type of filters as for concentration analyses (pre-filters: *Advantec* glass fiber filters GF-75 or GC-50 with pore size 0.7 μm and 1.2 μm, respectively, and a 0.22 μm *Advantec* Mixed Cellulose Ester Membrane filter). In September 2006 and August 2007 we used an anaerobic pressure filtration apparatus with N_2 overpressure to minimize oxidation. Vacuum filtration was used in June 2006. Most particulate Mo was captured by the pre-filter (termed here *particulate Mo*), and we confirmed that Mo in filtered water plus Mo on the pre-filter matched the Mo content in unfiltered water samples (Fig. 2e,f). Filtration commenced within seven hours of sampling. The water samples were acidified to a pH of 1–2 with a few milliliters of doubly distilled concentrated HNO_3. Particulates were leached from the filter in

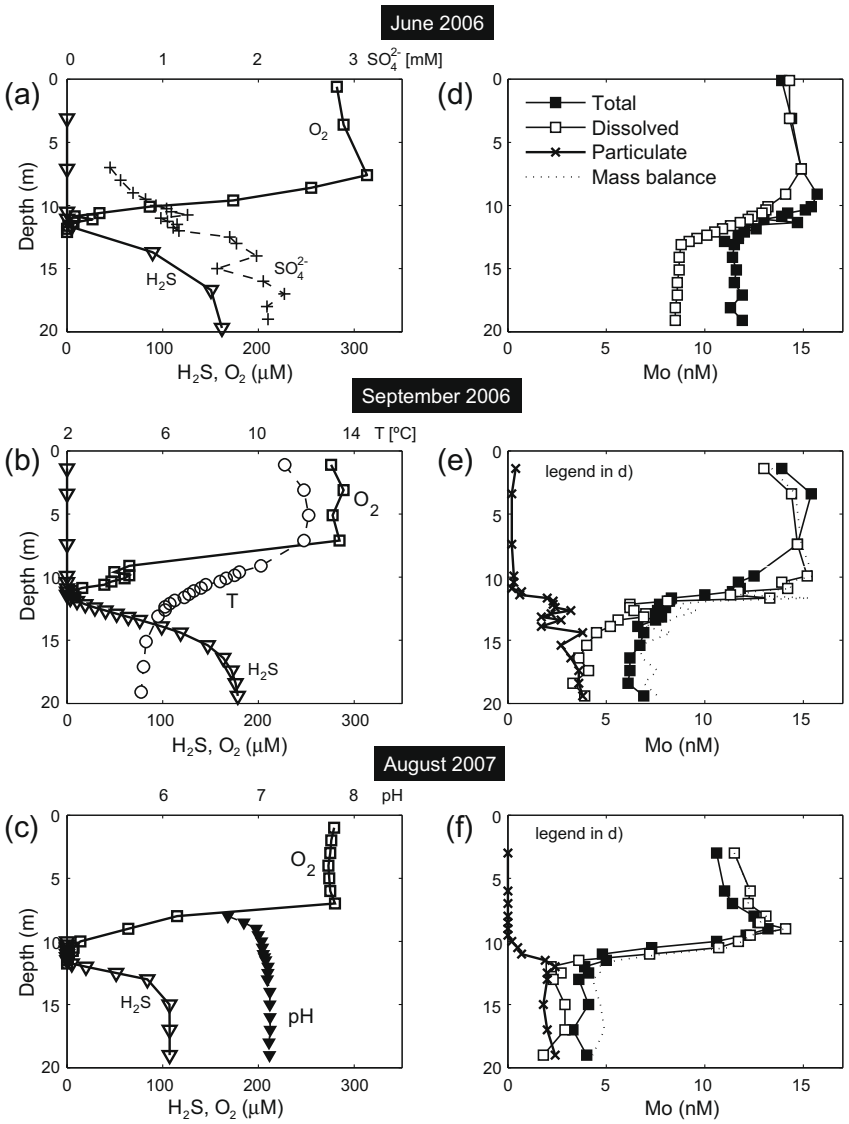

Fig. 2. The main chemical and physical characteristics of Lake Cadagno water column are shown in panels (a–c) for three sampling periods. Depth profiles showing O_2 (□) and molybdate-reactive H_2S (▽) concentrations are shown in units of μM (NB! Total sulfide concentrations are a factor of ~2 higher: $\Sigma S^{2-} = H_2S + HS^- + S^{2-}$). The salinity increases with depth and is inversely correlated to O_2 (not shown). This causes a density increase and thus permanent stratification throughout the year. The sulfate concentration profile from June 2006 (+) is shown in millimolar in panel (a), the temperature profile for September 2006 (○) is shown in °C in panel (b) and pH (▼) is shown in panel (c) for August 2007. The annual changes in the sulfate profile are small (Tonolla et al., 2003), temperature varies only in the mixolimnion (surface is frozen in the winter, 8.6 °C at 3.6 m depth in June 2006) and pH varies between 6.9 and 7.9 at 11 m depth and remains close to neutral at greater depths. The turbidity peaks at the chemocline which indicates the highest density of cells (not shown). In panel (d–f) Mo concentrations of unfiltered water/total Mo (■), filtered water/dissolved Mo (□) and filter/particulate Mo (×). Filtrate concentrations from June were not measured. The Mo control curve (dotted line) shows that $[Mo]_{total} = [Mo]_{diss} + [Mo]_{part}$ holds within precision of the analyses.

2N HNO_3. About 1 L filtered lake water, containing from 400 to 1400 ng Mo, was evaporated for each depth and the residue treated with hydrogen peroxide and aqua regia to oxidize "dissolved" organic matter. The total Mo procedural blank for water samples using Millipore 18.2 MΩ H_2O (including pumping, filtration, purification and sample handling through all procedures) contained ~10 ng Mo, enabling us to analyze samples with >250 ng Mo with a negligible blank contribution.

Precipitation was sampled as snow in June 2006, and in 1 kg evaporated snow, Mo was below the detection limit (<0.1 pM). We conclude that precipitation is a negligible source of Mo to the lake. Rock samples of dolomite and granite were collected from outcrops near the lake (Fig. 1) and crushed to fine powders in a clean agate mortar.

We installed sediment traps at depths of: 7, 9, 12, and 17 m and collected them after 54 days (August 30–October 23, 2007). These were constructed by attaching a funnel to

acid-washed polyethylene bottles and suspended in triplicate at each depth. Unfortunately, the funnels retained the sediment at the edge and thus acted to inhibit particle capture, so sediment flux rates could not be calculated, because the effective capture area is unknown (but smaller than the cross-sectional area of the trap). The content of each trap was filtered through a 1.2 μm Advantec GC-50 glass fiber and a 0.22 μm *Advantec* Mixed Cellulose Ester Membrane filter, so that both small and large particles could be analyzed. Particles in the traps are termed *sinking particles*.

Sediments were collected with a sediment coring device lined with a removable plastic sleeve. Cores were plugged with stoppers to avoid oxygenation and kept vertical until cut in slices and stored in 50 ml centrifuge tubes. Pore water was separated from the sediment in a centrifuge for 15 min at 3000 rpm and filtered through Advantec GC-50 glass fiber filters with a nominal pore size of 1.2 μm.

3.2. Analytical techniques

Oxygen was measured by Winkler titration (Winkler, 1888) with a detection limit of <1 μM, while sulfide concentrations were measured with Cline reagent (Cline, 1969) with a detection limit <1 μM. Conductivity and turbidity were measured with a *YSI 6000 multiparameter probe* from *YSI Hydrodata Ltd.*, while pH was measured with a calibrated pH meter. Sulfate concentrations were measured by ion chromatography on a *Sykum* ion chromatograph with column suppression. Uncertainty was <5%.

The water content of the sediment was measured by mass difference before and after drying the sample in an aluminum tray for 24 h in a kitchen oven at 110 °C. This was done immediately after sampling to minimize potential dehydration before the initial weighing. Samples were cooled in a desiccator to ensure no mass gain during cooling. Determination of the sedimentary burial flux of Mo is very sensitive to accurate estimates of the sedimentary water content (porosity), so three different cores were compared to guarantee robust results.

The organic C wt% was calculated from the weight lost during ignition (Loss on Ignition, LOI) of the dry sediment for 24 h at 550 °C assuming the average composition of organic matter is CH_2O (0.4 g C per gram lost weight). Two different cores were measured to check the consistency of the results. Total trace metal concentrations were obtained from samples ashed in ceramic crucibles to avoid metal contamination. Samples were brought into solution by a series of consecutive acid digestions including concentrated $HF + HNO_3$, HCl, and HNO_3. The dissolved sediment was diluted with MQ H_2O to a 0.32 M HNO_3 solution. All metal concentrations were determined with a quadropole inductively coupled plasma mass spectrometer (ICPMS) by intensity comparison to a multi-element calibration curve with correction for plasma suppression using a multi-element internal standard.

3.2.1. Sr and Mo isotopic compositions

Sr was purified from 2 ml filtered water, dried, redissolved in nitric acid, and processed over miniature columns charged with 200 μL of *Eichrom's SrSpec™* resin using a standard elution scheme (Horwitz et al., 1992). Sr isotopic compositions were measured on a *VG-54 Sector* multiple-collector Thermal Ionization Mass Spectrometer (TIMS) at the Institute of Geography and Geology, University of Copenhagen in dynamic collection mode. $^{87}Sr/^{86}Sr$ ratios were normalized to $^{86}Sr/^{88}Sr = 0.1194$. Procedural blanks were below 150 pg and they were negligible relative to the amount of sample Sr. The long-term reproducibility of the NBS 987 Sr standard for our method is $^{87}Sr/^{86}Sr = 0.710235 \pm 0.000017$ (2 SD; $n = 28$).

For Mo isotopes, rock samples were dissolved in 6 M HCl after a $HF–HNO_3$ digestion while water samples were evaporated to reduce volume first. Samples were purified using the separation method described in Barling et al. (2001) for analysis using an element spike to correct for instrumental mass bias. The water samples from September 2006 contained organic matter which blocked fluid flow in the columns reducing chemical recovery during purification. Hence, profiles from September 2006 and August 2007 were also purified by batch separation using Biorad chelating resin Chelex-100 after equilibration with a $^{97}Mo–^{100}Mo$ double spike for 48 h prior to extraction. The recovery of this methodology was ~80%, and we assumed an exponential mass bias law to apply to both the instrumental fractionation and the loss during purification. The element spike and double spike methods were compared to check that the two techniques give consistent isotope compositions. The data for the same waters sampled in August 2007 analyzed with both methods give consistent results (Table 1, Fig. 3). All samples were oxidized with hydrogen peroxide prior to isotope analysis to remove organics eluted from the resin.

Samples of sediment-trap material were analyzed using a $^{97}Mo–^{100}Mo$ double spike to correct for mass bias in the instrument and on the columns (Siebert et al., 2001), since samples prepared by element spike (Barling et al., 2001) suffered from low-yield during purification.

The stable isotope compositions of molybdenum were determined with a *Thermo-Fisher Scientific Neptune* multiple-collector inductively coupled plasma mass spectrometer (MC-ICPMS) at Arizona State University. Instrumental mass bias for the non-double spiked samples was corrected for by standard-sample bracketing and an external Zr spike technique (Barling et al., 2001). The mass spectrometer was set up to measure ^{90}Zr, ^{91}Zr, ^{92}Mo ($+^{92}Zr$), ^{95}Mo, ^{96}Mo ($+^{96}Zr$), ^{97}Mo, ^{98}Mo and ^{100}Mo from which we could derive five Mo isotope ratios and one Zr isotope ratio; the latter was used to correct for instrumental mass bias. Data was only accepted when maximum and minimum of δ/amu for $\delta^{92}Mo$, $\delta^{98}Mo$ and $\delta^{100}Mo$ differed by $\leqslant 0.1‰$ per amu ($\delta^{x}Mo = [(^{x}Mo/^{95}Mo)_{sample}/(^{x}Mo/^{95}Mo)_{standard} - 1] \times 10^3$). Data was also rejected if the mass bias corrected $\delta^{98}Mo$ differed from $\delta^{98}Mo$ obtained from standard-sample bracketing by more than 0.50‰, suggesting that significant correction for matrix effects was required. In addition, in-house rock and gravimetric standards were run repeatedly in each session to verify agreement with long-term averages. Three well-known standards were processed through chemical purification (SDO-1, Nod-A1, and Nod-P1) to verify that the methods were consistent with previous work (Barling

Table 1
Mo concentrations measured by isotope dilution at Arizona State University and $^{98}Mo/^{95}Mo$ isotope fractionation relative to the RochMo2 standard (2 SD uncertainty levels) given in nmol kg^{-1} and ‰, respectively. The precision on $\delta^{98}Mo$ of the mass spectrometric analyses is typically 0.05‰ (2 SE). Error bars represent the 2 SD reproducibility of each sample measured on different days, typically 0.14‰ (2 SD) and *n* is the number of replicate analyses. Data for complete replicate digests are shown as separate rows.

Description	Depth (m)	$[Mo]_{diss}$ (nmol kg^{-1})	$\delta^{98}Mo$ (‰)	*n*[a]	Technique[b]/Yield (%)	Sr (μmol/kg)	$^{87}Sr/^{86}Sr$[c]
June 2006[d]							
Oxic water	3.0	14.3	0.78 ± 0.16	3	100 ± 1%	12.7	0.708082
Replicate 2	3.0	14.3	0.91 ± 0.02	2	100 ± 1%	12.7	0.708082
Replicate 3	3.0	14.3	0.97 ± 0.07	3	98 ± 1%	12.7	0.708082
Replicate 4	3.0	14.3	0.90 ± 0.18	3	DS	12.7	0.708082
Oxic water	7.0	14.9	0.95 ± 0.05	4	98 ± 2%	16.8	0.708058
Oxic water	9.8	13.0	1.29 ± 0.17	3	98 ± 2%	34.2	0.707994
Oxic water	10.4	12.2	1.37 ± 0.07	3	99 ± 2%	36.1	0.707972
Chemocline	11.0	10.9	1.45 ± 0.14	4	98 ± 2%	42.5	0.707966
Sulfidic water	13.0	8.8	1.61 ± 0.14	4	96 ± 2%	53.2	0.707961
Sulfidic water	16.0	8.6	1.74 ± 0.17	6	100 ± 2%	54.8	0.707936
Sulfidic water	16.0 particulate		1.34 ± 0.27	3	88 ± 1%		
Sulfidic water	19.0	8.5	1.71 ± 0.13	2	97 ± 1%	55.7	0.707956
Riverine inlet	0.0	8.0	0.86 ± 0.20	4	98 ± 2%	0.12	0.720920
Swamp inlet	0.0	32.2	0.78 ± 0.03	3	99 ± 1%	0.49	0.717748
Riverine outlet	0.0	14.3	1.02 ± 0.10	3	98 ± 1%		
September 2006							
Oxic water	3.4	14.4	0.89 ± 0.13	2	DS	12.3	0.708090
Replicate	3.4	14.4	0.91 ± 0.17	2	DS		
Replicate	3.4	14.4	1.00 ± 0.19	3	DS		
Replicate	3.4	14.4	0.92 ± 0.28	3	103 ± 2%		
Oxic water	10.4	13.9	1.10 ± 0.18	2	DS	30.2	0.707993
Oxic water	10.9	14.2	1.08 ± 0.04	3	DS	32.5	0.707987
Chemocline	11.2	11.7	1.09 ± 0.15	3	DS	37.3	0.707978
Chemocline	11.4	11.3	1.46 ± 0.12	3	DS	39.5	0.707968
Chemocline	11.7	13.3	1.67 ± 0.20	2	DS	42.5	0.707971
Sulfidic	12.4	6.2	2.35 ± 0.05	3	DS	50.6	0.707955
	13.4 Particulate						
Sulfidic			1.16 ± 0.06	2	99 ± 3%		
	14.3 Particulate						
Sulfidic		8.8	1.33 ± 0.08	3	99 ± 3%		
Sulfidic	16.4	3.6	2.82 ± 0.004	2	DS	47.0	0.707968
Sulfidic	19.4	6.2	1.51 ± 0.09	3	DS	50.1	0.707949
Riverine inlet	River in	–	0.87 ± 0.08	3	DS		
Riverine outlet	River out	–	0.86 ± 0.11	3	DS		
August 2007							
Oxic water	7.0	12.2	0.92 ± 0.10	4	77 ± 3%	12.9	
Oxic water	7.0	12.2	0.93 ± 0.10	2	DS	12.9	
Oxic water	9.0	14.1	0.93 ± 0.11	3	96 ± 3%	23.2	
Oxic water	9.0	14.1	0.99 ± 0.10	2	DS	23.2	
Oxic water	10.3	10.7	1.00 ± 0.19	3	95 ± 1%	27.4	
Oxic water	10.3	10.7	1.10 ± 0.10	2	DS	27.4	
Oxic water	11.0	7.2	1.27 ± 0.26	5	99 ± 9%	28.8	
Oxic water	11.0	7.2	1.32 ± 0.08	2	DS	28.8	
Chemocline	11.8	2.2	1.49 ± 0.12	4	93 ± 4%	29.8	
Chemocline	11.8	2.2	1.23 ± 0.17	2	DS	29.8	
Chemocline	12.1	2.7	1.32 ± 0.18	4	107 ± 9%	29.6	
Chemocline	12.1	2.7	1.49 ± 0.06	1	DS	29.6	
Sulfidic water	12.5	2.7	1.68 ± 0.09	3	93 ± 3%	30.9	
Sulfidic water	12.5	2.7	1.88 ± 0.16	1	DS	30.9	
Sulfidic water	15.0	2.9	1.61 ± 0.23	4	98 ± 7%	31.2	

(*continued on next page*)

Table 1 (*continued*)

Description	Depth (m)	$[Mo]_{diss}$ (nmol kg^{-1})	$\delta^{98}Mo$ (‰)	n[a]	Technique[b]/Yield (%)	Sr (μmol/kg)	$^{87}Sr/^{86}Sr$[c]
Sulfidic water	15.0	2.9	1.84 ± 0.05	2	DS	31.2	
Sulfidic water	19.0	1.8	1.72 ± 0.04	3	$102 \pm 3\%$	31.8	
Sulfidic water	19.0	1.8	1.76 ± 0.12	2	DS	31.8	

[a] Number of replicate measurements of $\delta^{98}Mo$ from which the reproducibility is derived as 2 SD of the mean.
[b] Methods applied to correct for instrumental mass bias are either quantitative extraction (>92% yield) or doping with double spike (DS) prior to purification.
[c] Sr isotope compositions measured by TIMS, the long-term producibility of the NBS 987 Sr standard for our method is $^{87}Sr/^{86}Sr = 0.710235 \pm 0.000017$ (2 SD; $n = 28$).
[d] Waters sampled in June 2006 are filtered using aerobically using a vacuum pump, while September and August samples are filtered anaerobically using pressure filtration in a N_2 atmosphere.

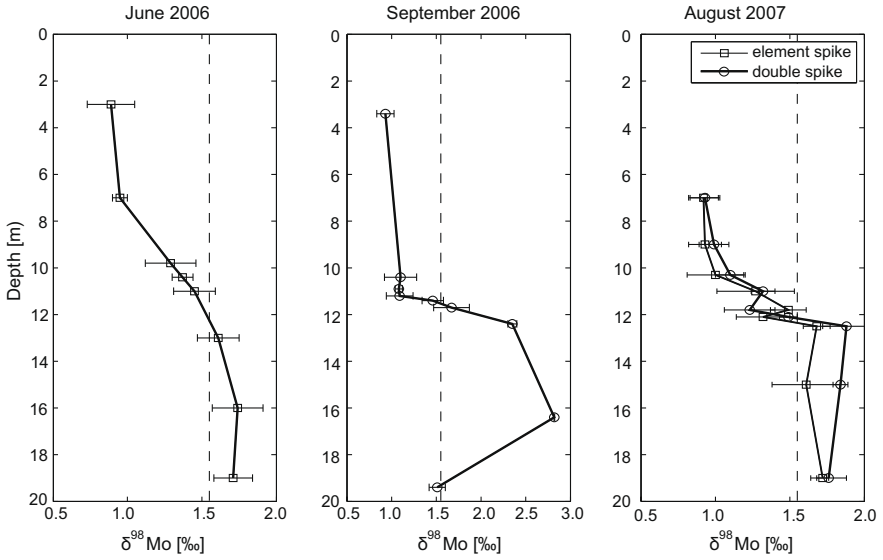

Fig. 3. Mo isotopic composition in the water column expressed as $\delta^{98}Mo$ in permil of the dissolved water. Data from (a) June 2006, (b) September 2006 (c) August 2007. Instrumental mass bias correction is made by either the Zr-doping technique (□) or double spike technique (○) also indicated in Table 1. Notice the different scale in b). Dashed lines represent the subaquatic (dolomitic) value.

et al., 2001; Siebert et al., 2001). Accuracy of the measurements was monitored by measurements of an ICP standard and the SDO natural sample by adding a gravimetrically measured amount of calibrated ^{95}Mo spike to result in a −1‰ offset on $\delta^{97}Mo$.

For data presentation, we use the Zr-corrected $^{98}Mo/^{95}Mo$ ratio and compare to the average of the ASU in-house standard "RochMo" (Alfa Aesar Specpure Lot # 802309E run immediately before and after each sample; standard-sample bracketing). Errors are reported as the 2 SD reproducibility for replicate analyses of the same sample. The long-term reproducibility of the USGS rock standard SDO-1 is 0.15‰ (2 SD; $n = 255$) over a period of 3 yrs. The beam intensity was enhanced by at least a factor of eight using an Apex nebulizer compared to wet aspiration, making it possible to analyze solutions with 40 ppb Mo at ^{97}Mo intensities of ~250 mV.

Chemical yields for Mo during column separation were measured for all non-double spiked samples by isotope dilution using a calibrated ^{97}Mo spike on pre- and post-chemistry aliquots. This technique allows for precise yield determination because the $^{97}Mo/^{95}Mo$ isotope ratio could be measured to a precision of <1%. In most cases, mass-dependent isotope fractionation during purification was negligible due to a 'near'-quantitative yield (>92%).

For the double-spiked samples, the instrument was set up to measure ^{92}Mo, ^{94}Mo, ^{95}Mo, ^{96}Mo, ^{97}Mo, ^{98}Mo, ^{99}Ru, and ^{100}Mo. All seven isotopes allow correction for instrumental mass bias and isobaric interferences with Zr (^{92}Zr, ^{94}Zr, and ^{96}Zr) simultaneously. Our data reduction procedure utilized a least squares fit with six equations (measured ratios) to four unknown parameters: instrumental mass bias (F_{ins}), natural isotope fractionation (F_{nat}), spike/sample molar ratio (x) and Zr/Mo molar ratio (z). The seven equations can be written in index notation $(^{i}Mo/^{92}Mo)_{measured} = ((^{i}Mo/^{92}Mo)_{std} \cdot m^{-Fnat} + x \cdot (^{i}Mo/^{92}Mo)_{spike} + z \cdot (^{i}Zr/^{92}Zr))m^{-Fins}$, where index i represent any of the isotopes. The optimal solution is found using a MATLAB® optimization procedure created by Stephen Romaniello at Arizona State University.

A preliminary data quality check was performed prior to the double spike data reduction by rejecting lines of data (1 line = data integrated over 3 s) with low signal to noise ratio, $^{95}Mo < 0.1$ V. An approximate solution to the mass bias corrected Mo isotope distribution was derived and lines were rejected if the isotope distribution failed to follow an internally consistent mass fractionation law (cyclic rejection of outliers with any isotope ratio outside 3 SD of the mean of remaining lines). The δ^{98}Mo was derived from the mean of 30 lines and additional quality check included a rejection of the sample data if all lines did not converge in the data reduction and if the standard error of the mean δ^{98}Mo value was 3 times greater than for a standard (0.10‰) or 10 times greater than the expected error based on counting statistics alone. The misfit between predicted and observed isotope ratios were calculated for each isotope ratio and termed 'residues'. We rejected data if the infinity norm of Zr-free residues (^{95}Mo, ^{97}Mo, ^{98}Mo, and ^{100}Mo) exceeded the error expected from counting statistics, and if the derived instrumental mass bias varied by more than 5% from a standard. All samples were spiked with 10–90% Mo (by moles) which is known to give correct results in spiked standards. We calculate the δ^{98}Mo value by subtracting the mean of the daily standards to correct for changes in fractionation behavior in the instrument between different days. Finally, we analyzed a known rock standard (SDO-1) to ensure accurate results. SDO-1 was found to have $\delta^{98}Mo = 1.13 \pm 0.07$‰ (2 SD; 9 sessions) which is in excellent agreement with the results obtained by Zr-doping, $\delta^{98}Mo = 1.14 \pm 0.14$‰ (2 SD; 65 sessions).

4. RESULTS

4.1. General chemical characterization of the water column

Dissolved oxygen, total sulfide (ΣS^{2-}) and conductivity profiles are shown in Fig. 2a–c. The water column was saturated with O_2 down to a depth of 7 m, followed by a decrease towards the chemocline. Sulfate is delivered horizontally by subaquatic springs to the deep lake, and the concentration decreases towards the oxic zone and into the sediment. Sulfide starts to accumulate at 11–12 m, just below the steepest conductivity gradient, and reached a maximum concentration of about 250 μM at depth in the water column (Del Don et al., 2001; Peduzzi et al., 2003; Tonolla et al., 2003). For our purposes, 'chemocline' refers to the narrow anoxic zone where the sulfide concentration begins to increase.

The water column ΣS^{2-} profile can be fitted to sigmoidal functions of depth. The steepest gradients of these functions give consistent results for all field trips at 100–150 μM/m. In September 2006 and August 2007, the chemocline was located deeper compared to June 2006 (Fig. 2a–c) correlating with steeper sulfide gradients at these times.

Water column pH was measured in August and increased from 6.9 to 7.1 in going from 8.5 to 19 m (Fig. 2c). The precision on the pH meter was <0.1 units. Values up to pH = 7.9 have previously been observed within the oxic waters but it remains close to our measured value of 7.1 in the sulfidic zone (Del Don et al., 2001).

4.2. Molybdenum in the sulfidic water column

The concentration of dissolved Mo decreased by 40–80% (June 2006: 40%, September 2006: 70% and August 2007: 80%) across the chemocline into the sulfidic waters. A substantial fraction (30–60%) of the Mo in the sulfidic zone was adsorbed or complexed with suspended particles recovered from 1.2 μm glass fiber filters (Fig. 2d–f, EA-Table A1 in electronic annex A). Our results confirm that dissolved Mo plus particulate Mo equals total Mo within error. There is considerable chemical enrichment of Mo in the sediments of the deep basin: these sediments are 2–3 orders of magnitude elevated in Mo concentration (Table 5) compared to typical rocks in the catchment area (i.e., dolomite and gneiss contain <1 ppm Mo, Table 2).

The isotopic composition of Mo varied in the water column (Table 1, Fig. 3). The sulfidic water at 19 m was enriched in heavy Mo isotopes, with $\delta^{98}Mo = 1.73 \pm 0.05$‰ in June 2006 and August 2007 compared to the well-mixed mixolimnion with $\delta^{98}Mo = 0.91 \pm 0.11$‰ ($2\sigma$, 10 samples) at 3–7 m depth. In September 2006, intermediate sulfidic waters were dramatically shifted to δ^{98}Mo values of up to 2.8‰, which decreased towards the sediment value at depth. The main river source to the lake carried ~8 nM Mo with $\delta^{98}Mo = 0.86 \pm 0.20$‰. The swamps in the catchment area had variable Mo concentrations; one sample taken north of the lake contained as much as 32 nM Mo with $\delta^{98}Mo = 0.78 \pm 0.03$‰. This is within error of the isotopic composition of the riverine source. The main outlet contained ~14 nM, with $\delta^{98}Mo = 1.02 \pm 0.10$‰ equivalent, within error, to the oxic waters. These surface waters

Table 2
Mo and Sr concentrations and isotope composition in rocks from the catchment area.

Name	Rock type	[Sr][a] (ppm)	$^{87}Sr/^{86}Sr$	n_{Sr}[b]	[Mo][a] (ppm)	$\delta^{98/95}$Mo (‰)	n_{Mo}[c]	Yield (%)
Dol1	Dolomite	633 ± 61	0.70773 ± 0.00001	17	0.48 ± 0.04	1.56 ± 0.10	5	94 ± 2
Dol2	Dolomite	277 ± 41	0.70784 ± 0.00004	15	0.32 ± 0.07	1.55 ± 0.06	4	93 ± 2
Gne1	Gneiss	114 ± 4	0.72840 ± 0.00001	16	0.28 ± 0.03			
Gne2	Gneiss	38 ± 1	0.73645 ± 0.00001	13	0.15 ± 0.001			

[a] Measured on the Thermo-Fisher Scientific X-Series quadrupole ICPMS at Arizona State University by intensity comparison to a standard curve.
[b] Number of replicate analyses for $^{87}Sr/^{86}Sr$.
[c] Number of replicate analyses for $\delta^{98/95}$Mo measured on different days.

fall close to the weighted mean of major global rivers, $\delta^{98}Mo = 0.7‰$ (Archer and Vance, 2008).

4.3. Sr in the water column

The concentration of Sr increased with depth into the deep waters, reaching up to ~50 μmol kg^{-1} in the monimolimnion (Table 1). In contrast, the riverine inlet and swamps were relatively dilute (0.12 μmol kg^{-1} and 0.49 μmol kg^{-1}, respectively; Table 1). The Sr isotopic composition decreased with depth (Table 1) and $^{87}Sr/^{86}Sr$ correlates with 1/Sr (with a correlation coefficient of $R^2 = 0.98$ in both June 2006 and September 2006, Fig. B1 in electronic annex B). Typical rocks in the local environment displayed a significant variation in Sr concentration. Strontium is abundant in outcropping dolomites which strongly influence the chemistry of the monimolimnion (Table 2). The $^{87}Sr/^{86}Sr$ composition of the oxic surface water is dominated by diffusion from the deep lake, rather than the riverine source which is ~500 times more dilute. Also, of the potential source rocks in the catchment area, the isotopic composition of the Sr in the deep lake is closest to the dolomites. This strongly suggests that the main source of Sr to the deep lake is the dolomites, as input by subaquatic springs.

4.4. Molybdenum isotopes in catchment rocks

Since the dolomites provide Sr to the deep lake, we analyzed the Mo isotopic composition in nearby dolomite outcrops to evaluate the prospects of a subaquatic Mo source. Analyses of two dolomites revealed indeed $\delta^{98}Mo = 1.56 \pm 0.10‰$ and $1.55 \pm 0.06‰$ (Table 2) which is heavier than the riverine value. The concentration of Mo in two dolomites and two gneisses from the catchment area were found at 0.32 ppm, 0.48 ppm, 0.15 and 0.28 ppm, respectively (Table 2). This is 4–7 times lower than average upper crust (1.5 ppm, Taylor and McLennon, 1995).

4.5. Sinking particulates and suspended particulates

Pre-filters (>0.7 μm) from the 12 m sediment-trap were dark purple due to rain out of purple sulfur bacteria from the chemocline. The 17 m sample, in contrast, lacked this color and contained less sediment. Both 7 and 9 m traps contained very little sediment. Microscopic examination revealed only organic matter in the traps from the monimnolimnion and no metal sulfide particles (e.g. framboidal pyrite). For the particles caught in the sediment traps, Mo/Ti increased with depth. At 12 m depth Mo/Ti values of the large fraction were a factor of three higher than par-

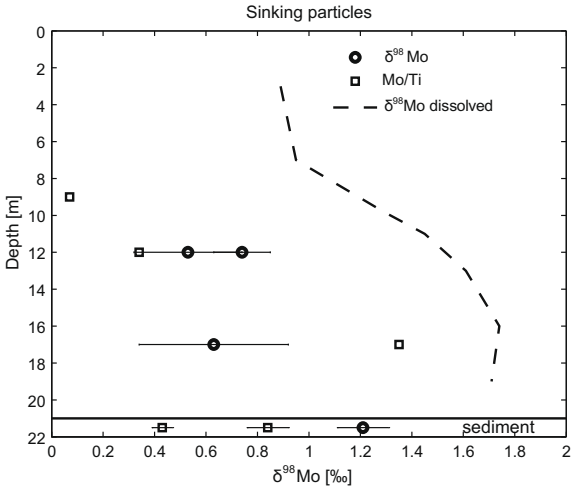

Fig. 4. Depth profile showing $\delta^{98}Mo$ (●) and Mo/Ti (□) in sediment traps. Sinking particles are offset by −0.8 to −1.2‰ relative to dissolved Mo (dashed line). Sediment values are shown below the horizontal line.

Table 4
$\delta^{98/95}Mo$ of sediment traps left hanging in the water column for 54 days.[a]

Name	Description (m)	$\delta^{98/95}Mo$ (‰)	*n*
ST54-3a1	Sediment-trap 12	0.53 ± 0.21	2
ST54-3b2	Sediment-trap 12	0.74 ± 0.11	3
ST54-4c1	Sediment-trap 17	0.63 ± 0.29	1

[a] Isotope analyses were performed by equilibrating sample and ^{97}Mo–^{100}Mo double spike prior to purification. Errors represent 2 SD reproducibility.

Table 3
Element distribution between small and large particles in the sediment traps.

Small particles 0.2–0.7 μm				Large particles >0.7 μm		
Depth m	Mo ng	Mo/Fe mg/g	Mo/Ti mg/g	Mo[a] ng	Mo/Fe mg/g	Mo/Ti mg/g
7	16	4.5	18.5	45	n.d.	–
9	28	2.2	18.7	24	0.2	7
12	68	3.0	37.6	4342	1.4	34
17	56	4.6	32.4	252	3.8	135
Blank filter	13	12.5	10.0	9	n.d.	–
Proc. blank	<1	45.3	15.1	<1	11.7	11.6
Sediment						
Sediment upper 8 cm June 2006 core J					3.2 ± 0.2 (1σ)	84 ± 8 (1σ)
Sediment upper 8 cm August 2007, core 1					3.0 ± 0.6 (1σ)	43 ± 4 (1σ)

[a] Approximate amount of Mo in one trap estimated from the amount of analyzed filtrate. The 12 m trap data is based on the analysis of three out of eight filters. One of the filters has 4 times more Mo than the other two and dominates the above average.

Table 5
Sedimentary Mo, Mo/Ti and $\delta^{98/95}$Mo.

Name	Depth (cm)	[Mo] (ppm)	Mo/Ti (mg/g)	$\delta^{98/95}$Mo (‰)	*n*
June 2006, core J, 21 m depth					
Sed2	2.5	132	82.6	–	–
Sed3	3.8	158	93.9	1.15 ± 0.29	5
Sed4	5.0	166	90.2	1.22 ± 0.12	3
Sed5	6.3	129	70.4	1.25 ± 0.15	3
Sed6	7.5	167	87.0	–	–
Sed7	8.8	180	81.3	–	–
Sed8	10.0	130	54.4	1.31 ± 0.10	3
Sed9	11.3	117	51.2	1.19 ± 0.14	3
Sed10	12.5	124	58.6	–	–
Sed11	13.8	58	25.6	–	–
Sed12	15.0	121	65.0	1.44 ± 0.09	3
Sed 14	17.5	123	42.6	1.37 ± 0.19	3
Sed 15	18.8	94	30.7	–	–
Sed16	20.0	–	–	0.98 ± 0.16	3
Sed17	21.3	7	2.2	0.87 ± 0.18	4
Sed18	22.5	5	1.3	1.11 ± 0.16	4
Aug 2007, core 1, 21 m depth					
Sed_a2	1.5	114	47.6		
Sed_a3	3.0	101	39.7		
Sed_a4	4.5	91	39.0		
Sed_a5	6.0	183	43.9		
Sed_a7	9.0	116	30.7		
Sed_a9	12.1	83	34.2		
Sed_a11	15.1	165	40.0		
Sed_a13	18.1	77	18.6		
Sed_a15	21.1	6	0.7		
Sed_a17	24.1	53	11.0		
Sed_a19	27.1	2	0.4		
Sed_a21	30.1	3	5.3		

ticles at 9 m depth and the procedural blank (Table 3), and by 17 m, the Mo/Ti of particles were ~20-fold higher than at 9 m depth and significantly higher than the sediment value for the largest particles and smaller than the sediment value for the smallest particles (Table 3, Fig. 4). The sediment traps at 12 m showed the lowest δ^{98}Mo values observed in the lake system at a mean value of 0.6‰. This isotopic offset is −0.3‰ relative to oxic waters and ca. −0.8‰ relative to dissolved Mo at the same depth. At 17 m the sinking particles carry similar δ^{98}Mo = 0.63‰, which is −1.2‰ lighter than dissolved Mo at the same depth and significantly lighter than the upper sediment (Table 4; Fig. 4). We also obtained data from particulate fractions. In June 2006 the suspended particles carried δ^{98}Mo = 1.34 ± 0.27‰ (2 SD; $n = 3$) compared to dissolved Mo δ^{98}Mo = 1.74 ± 0.17‰ (2 SD; $n = 6$) in the waters at 16 m depth. In September 2006, Mo associated with suspended particulates at 13.4 and 14.3 m depth carried 1.16 ± 0.06‰ (2 SD; $n = 2$) and 1.33 ± 0.08‰ (2 SD; $n = 3$), respectively, or ca. 1–1.5‰ lighter than dissolved Mo. In all cases particulate Mo was also lighter than deep water dissolved Mo, with a value similar to the sediment (Table 6).

4.6. Sediments and pore fluids

The sediment was black, finely laminated and smelled strongly of sulfide. The upper sediment was very fluid, containing ~98 wt% H_2O (Fig. 5a). The water content was measured on three separate cores, and the data are in good agreement.

Sulfate concentrations decreased from 2 mM in the overlying water to 1.3 mM in the uppermost few cm of sediment, with strongly decreasing concentration deeper into the sediment (Fig. 5a). Sulfide is produced by microbial sulfate reduction in the sediment and reached maximum concentrations of $\Sigma S^{2-} \sim 1000$ μM at 8 cm depth (Fig. 5). At greater than 8 cm depth, sulfide reacted out of solution, mostly as metal sulfides (Birch et al., 1996), but it remains above water column levels at 20 cm depth.

Table 6
Pore water [Mo] and δ^{98}Mo.

Name	Depth (cm)	[Mo] (μmol kg^{-1})	δ^{98}Mo (‰)	*n*	Column yield (%)
June 2006, Core J, 21 m depth					
LCJ_pw1	0	2116	1.60 ± 0.07	4	97 ± 2
LCJ_pw2	1.25	21			
LCJ_pw3	2.5	167			
LCJ_pw4	3.75	281			
LCJ_pw5	5	281			
LCJ_pw6	6.25	563	pw6 + pw7		
LCJ_pw7	7.5	1178	1.31 ± 0.28	4	89 ± 3
LCJ_pw8	8.75	792	pw8 + pw9		
LCJ_pw9	10	844	1.12 ± 0.10	3	95 ± 3
LCJ_pw10	11.25	1209	pw10 + pw11		
LCJ_pw11	12.5	2199	0.97 ± 0.21	5	95 ± 3
LCJ_pw12	15	2679	–		–
LCJ_pw14	16.25	3262	0.97 ± 0.03	5	99 ± 3
LCJ_pw15	17.5	2231	–		–
LCJ_pw16	18.75	3189	1.26 ± 0.06	3	97 ± 3
LCJ_pw17	20	1303	pw17 + pw18		
LCJ_pw18	21.25	2231	1.36 ± 0.16	3	99 ± 3

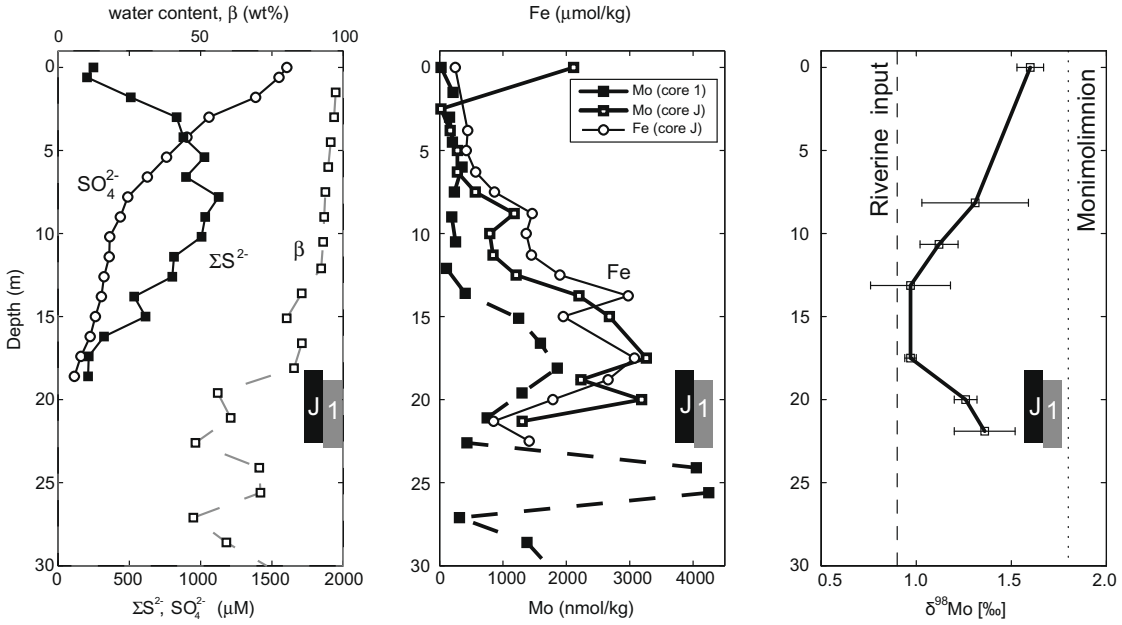

Fig. 5. Pore water characteristics in Lake Cadagno. Data comes from two cores sampled at the deepest point of the lake (21 m) in June 2006 (core J) and August 2007 (core 1). Panel (a) shows water content, β, in units of gram water per gram wet sediment (August 07) and concentrations ΣS^{2-} and SO_4^{2-} in μM (June 06). Panel (b) shows Mo concentrations and Fe (note the different axes). Panel (c) shows δ^{98}Mo of pore water. The dotted lines represent δ^{98}Mo values of the river (0.9‰) and monimolimnion (1.8‰). The turbidite deposits for core J and core 1 are marked with black and grey rectangular boxes, respectively.

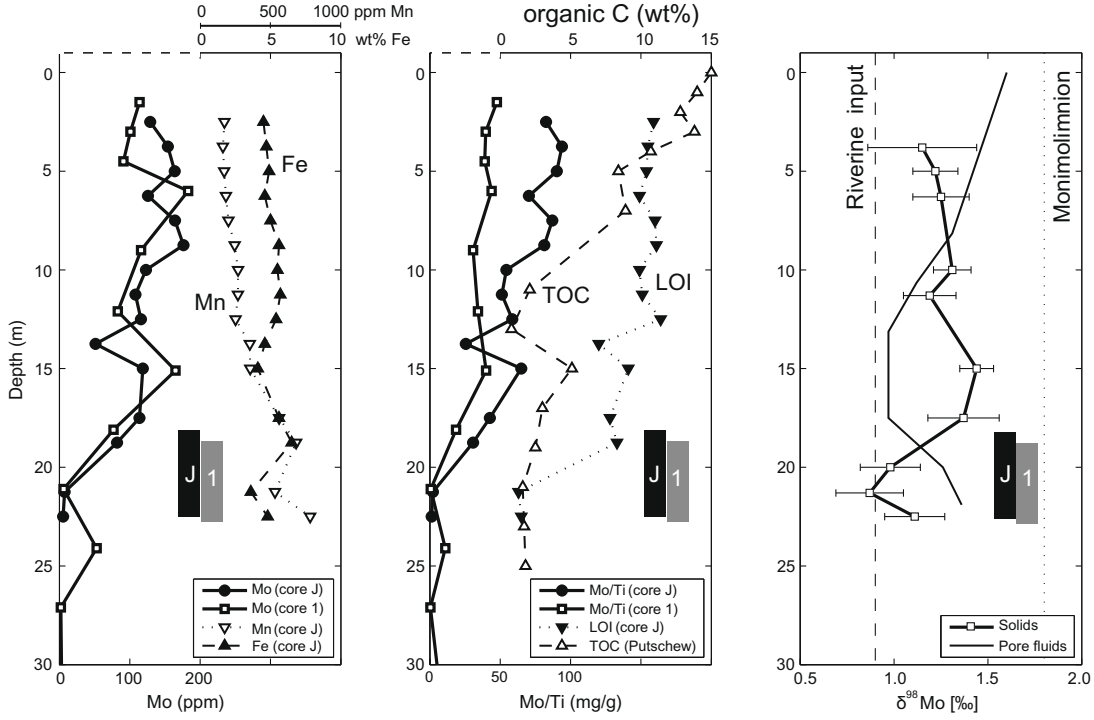

Fig. 6. Sediment characteristics in Lake Cadagno. Data comes from two cores sampled at the deepest point of the lake (21 m) in June 2006 (core J) and August 2007 (core 1). Panel (a) shows Mo in ppm, Fe (wt%) and Mn (wt%) (notice the different scale). Panel (b) shows Mo/Ti (mg/g) and organic C measured by LOI (this study) and TOC shown with '△' (Putschew et al., 1995). Panel (c) shows sedimentary δ^{98}Mo (‰). The dotted lines represent δ^{98}Mo values of the river (0.9‰) and monimolimnion (1.8‰) and the pore fluid δ^{98}Mo curve (thin black line) is shown for comparison. A linear fit in the sediment above the turbidite predicts a positive δ^{98}Mo trend with depth of 0.16 ± 0.05‰/10 cm ($R^2 = 0.64$). The turbidite deposits for core J and core 1 are marked with black and grey rectangular boxes, respectively.

The Mo concentration of dried sediment was ~130 ppm at the top of the core, declining by 10–20% to a depth of 19.6 cm, where a combination of lighter color, coarser grained texture, abruptly lower Mo/Ti, low water content and low organic matter concentrations indicate a turbidite deposit consistent with previous interpretations (Birch et al., 1996; Putschew et al., 1996). The top of the sediment contains 10.9 and 11.2 wt% total organic carbon for the cores sampled in June 2006 and August 2007, respectively. Previous studies using a TOC analyzer yielded similar values of 10–14 wt% (Putschew et al., 1995). Mo/Ti correlates with decreasing TOC (Fig. 6b) and depth profiles of Mo/TOC scatter around a value of 13 ± 2 and 11 ± 4 ppm/wt% for core J and core 1, respectively (Fig. 7). Sedimentary Fe is constant at 5.0 ± 0.7 wt% (Fig. 6a) and Mn concentrations increase with depth. None of these are correlated to sedimentary Mo (Fig. 6a). The sedimentary δ^{98}Mo profile scatters around 1.2‰ in the upper 10 cm, increasing to ~1.4‰ at 15 cm depth (Fig. 6c) with a strong decrease to 0.9‰ in the turbidite layer.

There is a profound enrichment of dissolved Mo and Fe in the pore waters (Fig. 5b). In June 2006, Mo concentrations increased to 1000 nM at the sulfide peak at 8 cm, and continued to increase to a maximum of over 3000 nM by 17 cm. In August 2007, even higher Mo concentrations were reached at depth, but concentrations remained relatively low until 15 cm, where a strong increase began. Dissolved Fe^{2+} from June 2006 mimics dissolved Mo concentration. The dissolved Mo/Fe molar ratio in the upper 8 cm was 0.31 ± 0.07. The δ^{98}Mo of dissolved Mo in the uppermost sediment layer were similar to the overlying water, and with depth, δ^{98}Mo decreased to values lower that the solid-phase Mo. In the turbidite deposit, solid-phase δ^{98}Mo was similar to Mo in the pore fluids.

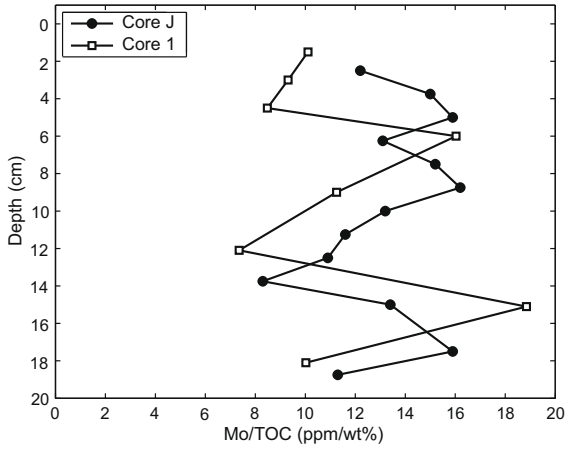

Fig. 7. Sedimentary Mo/TOC for core J sampled in June 2006 (●) and core 1 sampled in August 2007 (□). Both cores are sampled at the deepest point in the lake. Here, TOC is measured by loss on ignition (LOI). Linear fits of Mo (ppm) = $A \times$ Corg (wt%) + B (not shown) yields $A = 22.9 \pm 2.5$ and 17.7 ± 3.9 and ordinate-intercept $B = -21 \pm 16$ and -10 ± 23 with correlation coefficients $R = 0.86$ and 0.67 for core J and core 1, respectively.

5. DISCUSSION

In what follows, we consider the dynamics of Mo cycling within Lake Cadagno, with particular focus on the fractionations associated with Mo removal from the lake and into the euxinic sediments. These results allow us to assess in general how the isotopic composition of water column Mo is transferred to the euxinic sediments with implications for understanding the isotopic mass balance of the modern marine Mo cycle, and interpretations of the past.

5.1. Water column Mo

5.1.1. Concentration profile

The concentration gradient of dissolved Mo is steepest at the chemocline (Fig. 2) and suggests that substantial Mo removal occurs in the water column where sulfide concentrations are high. The drawdown of Mo into the sulfidic zone is from 40% to 70% of the overlying water concentrations ($Mo_{sulf}/Mo_{ox} = 0.3$ to 0.6, where 'sulf' and 'ox' represent sulfidic bottom water and oxic surface water, respectively). This magnitude of removal is comparable to that observed in Framvaren Fjord ($Mo_{sulf}/Mo_{ox} = 0.3$, $\Sigma S^{2-} \sim 6$ mM) and Lake Nitinat ($Mo_{sulf}/Mo_{ox} = 0.3$, $\Sigma S^{2-} \sim 150$ μM), but less dramatic than observed in the Black Sea ($Mo_{sulf}/Mo_{ox} \sim 0.06$, $\Sigma S^{2-} = 150$ μM) (Emerson and Huested, 1991). Clearly, Mo is also removed onto particles in the sulfidic waters of Lake Cadagno. This is evident from the accumulation of Mo onto sinking particles as seen by the progressively higher Mo/Ti ratios with depth (Fig. 4) resulting, near the bottom, in ratios similar to the sediments and much higher than particles in the oxic water column (Fig. 4; EA-Table A1). This observation contradicts previous studies which maintain that Mo is removed into sediments depositing in euxinic waters by processes below the sediment-water interface (Emerson and Huested, 1991; Crusius et al., 1996).

The removal process generates a concentration gradient causing a net flux of dissolved MoO_4^{2-} from the oxic mixolimnion into the sulfidic monimolimnion, where sulfidation to particle-reactive $MoO_{4-x}S_x^{2-}$ occurs (Erickson and Helz, 2000). The removal rate is slow enough that Mo resides ~80–130 days in the sulfidic zone (from flux calculations in Section 5.3). This time scale is much shorter than the water residence time of >1.5 yr (Electronic annex B) and is similar to the model predicted ~50–100 day characteristic time scale for molybdate conversion to trithiomolybdate at pH = 7.1 and H_2S = 100–190 μM without surface catalysts (Electronic annex C; Erickson and Helz, 2000). Consequently, the reaction kinetics of molybdate conversion to trithiomolybdate can explain the Mo residence time. As mentioned above, the rate of each successive sulfidation reaction is slower: $MoO_4^{2-} \leftrightarrow MoO_3S^{2-}$ (~5 h), $MoO_3S^{2-} \leftrightarrow MoO_2S_2^{2-}$ (~50 h), $MoO_2S_2^{2-} \leftrightarrow MoOS_3^{2-}$ (~60 days) and $MoOS_3^{2-} \leftrightarrow MoOS_4^{2}$ (~1.5 yrs) with increasing susceptibility for particle scavenging (Erickson and Helz, 2000). Indeed, laboratory experiments confirm that tetrathiomolybdate adsorbs with higher particle affinity than oxythiomolybdates onto both FeS_2 (Bostick et al., 2003) and FeS (Helz et al., 2004). Even though dis-

solved and particulate Mo will contain species with different degrees of sulfidation, tri-thiomolybdate must prevail given the Mo residence in the bottom waters of the lake (calculations in Electronic annex C). Thus, we propose that Mo is removed in the sulfidic waters primarily as tri thiomolybdate (Fig. 9). The degree to which the Mo species adsorb to particles is central to understanding the isotope fractionation expressed between particulate and dissolved Mo. This will be explored below.

5.1.2. Isotopes

The Mo concentration drop is associated with increasing δ^{98}Mo values in the dissolved pool, while for the sinking particles, Mo is ca. 0.8–1.2‰ lighter than their respective waters (Table 1). This suggests removal of preferentially lighter Mo isotopes from the sulfidic waters. Sediment δ^{98}Mo of about 1.2‰ is 0.6–2.2‰ depleted compared the dissolved Mo in the sulfidic zone (about 1.8‰; Figs. 3 and 4), suggesting a fractionation factor in excess of −0.6‰ operates in the water column as particles scavenge Mo in the sulfidic zone. Taken together, these observations confirm that isotope fractionation occurred while Mo was scavenged in the sulfidic water column.

The magnitude of isotope fractionation can also be evaluated from the depth trends in dissolved water column δ^{98}Mo values, provided that the Mo draw down (40–80%) is responsible for the +0.9‰ excursion in the dissolved phase compared to a source in the overlying oxic waters. The fractionation factor associated with that process is $^{98}\Delta = -1.7 \pm 0.6‰$ or $^{98}\Delta = -1.2 \pm 0.6‰$ following an equilibrium fractionation law and a Rayleigh fractionation law, respectively. These values are somewhat higher than those estimated from the δ^{98}Mo of the sinking particles (0.8–1.2‰, see above). This discrepancy could reflect an additional heavy groundwater Mo source (the δ^{98}Mo of the dolomitic limestone is 1.55‰) which could increase the steepness of the δ^{98}Mo gradient in through the chemocline and into the deep lake, yielding a higher apparent fractionation factor (the subaquatic source is discussed further in Electronic annex B).

Isotope fractionation during the ligand-exchange reactions accompanying the conversion of molybdate to thiomolybdate (Tossell, 2005) through successive sulfidation steps (e.g. MoS_4^{2-} relative to $MoOS_3^{2-}$) are predicted to impart about a −1.7 to −1.4‰ offset in isotope composition and there is an overall isotopic difference of −6.2‰ between tetrathiomolybdate and molybdate at Lake Cadagno temperatures. As discussed above, it is likely that less sulfidated oxythiomolybdates exist in so low abundance either in solution or on the particles, and that the isotope fractionation associated with those species would not be expressed. Accordingly, the degree of isotope fractionation observed between sinking particles and the sulfidic waters depends on the distribution of the thio-species in the water column and the reactivity of these species with particles.

We argue that given the likely distribution of thiomolybdate species in the lake, a 1.2‰ fractionation between water column molybdenum and the particles is realistic. For example, the −1.2‰ offset would be generated if the particles contained ~70% $MoOS_3^{2-}$ (assumed −1.7‰ relative to trithiomolybdate) and ~30% $MoO_2S_2^{2-}$ and the dissolved pool was 100% $MoO_2S_2^{2-}$. In this scenario, $MoOS_3^{2-}$ is preferentially reacted from solution onto particles, yielding a low abundance in the dissolved phase but a high abundance on the particles. As mentioned above, this scenario is consistent with the enhanced reactivity of more sulfidated species as observed in laboratory experiments of particle adsorption onto iron sulfides (Helz et al., 2004). Such enhanced reactivity of MoS_4^{2-} and $MoOS_3^{2-}$ might also be the case for Mo adsorption onto organic matter and humic acids. In a similar way, isotopic offsets is established in systems with di-thiomolybdate and tri-thiomolybdate.

5.2. Sediments

5.2.1. Sediment concentrations in solution and solid-phase

Mo is released from its particle carrier in the sediment with Mo increasing from 2 to 8 nM at the sediment-water interface to 2000–4000 nM at ~15 cm depth. This dramatic buildup would support the diffusion of Mo out of the sediment and back into the water column. In combination with decreasing solid-phase Mo (and Mo/Ti) with depth, our results provide evidence that Mo is mobilized and transported from the deeper sediments towards to the sediment surface. This behavior provides strong evidence that a majority of the particulate Mo is deposited as Mo^{VI} and is not reduced to insoluble Mo^{IV} and subsequently sequestered as molybdenite (MoS_2) even though this reaction is energetically favorable; $\Delta G^0 = -314.3$ kJ/mol (Bostick et al., 2003). Therefore, we see little evidence for biological removal mechanisms such as dissimilatory molybdate reduction (Tucker et al., 1998a,b).

Mo is released into pore fluids as organic carbon is oxidized (Figs. 5 and 6), resulting also in a decrease in solid-phase Mo concentration with depth (Fig. 6) and a relatively constant Mo/TOC with depth (Fig. 7). Organic carbon oxidation is driven by dissimilatory sulfate reduction above 8 cm, and methanogenesis below (Electronic annex B, Fig. B3). Increases in "dissolved" Mo and loss of solid-phase Mo may also accompany the conversion of FeS to pyrite with depth in the sediment, if FeS also acts as an important Mo carrier in the sediment. (Birch et al., 1996). Once in solution, Mo is likely bound and transported by diffusion as humic complexes. The sediment pore waters are a deep brown color, and this material precipitates on acidification indicating large quantities of humic acids. Indeed, in the anoxic and mildly sulfidic meromictic Lake Pavin, France, Mo is found to diffuse from the sediments (Viollier et al., 1995) in association with complex humic substances (Alberic et al., 2000).

The EXAFS adsorption spectra of Mo and humic acids complexes are quite similar to the spectral type observed in black shales (Helz et al., 1996), suggesting that the Mo in many cases is fixed in shales in an organic association (via Mo═O double bonds) and the data also indicates Fe—Mo interactions. Our interpretation of the Mo behavior in Lake Cadagno is consistent with these observations.

The geological rock record provides numerous examples of euxinic sediments displaying consistent Mo/TOC relationships (Algeo et al., 2007; Anbar et al., 2007). These

consistent relationships in a given setting imply that Mo was mainly transported to the sediments with organic matter with a consistent Mo/TOC ratio for the settling particles. Variability in the Mo/TOC between settings implies variability in the Mo/TOC of sinking particles. We find 12 ppm Mo/wt% TOC in Lake Cadagno (Fig. 7), which is typical for semi-restricted modern marine euxinic sediments such as Framvaren fjord (9 ppm/wt%), and lower than average for Phanerozoic black shales (27 ppm/wt%) (Scott et al., 2008). The diagenetic remobilization of Mo as we see in Lake Cadagno has not altered the Mo/TOC at depth, and therefore the Mo/TOC relationship in ancient shales can reflect a water column signature even through terminal stages of early diagenesis. This will be true as long as the organic carbon oxidized in a given setting is a rather constant proportion of that originally deposited, a rather constant proportion of Mo is removed during diagenesis and if the particles rain to the sediment with a rather constant Mo/TOC ratio. In marine settings, this Mo/TOC ratio is interpreted to reflect organic matter burial rate relative to bottom water Mo concentrations (Algeo et al., 2007) and is correlated to hydrographic conditions of deep water renewal rates (or accordingly restrictedness of the basin).

5.2.2. Mo isotopes in sediment pore fluids and its solid-phases

The δ^{98}Mo offset between sediments and pore fluids is ~0.5‰ at 12–17 cm depth where Mo release is most pronounced (Fig. 6). The release of light Mo into the pore fluids and out of the sediment by diffusion leaves the sediment at depth with an apparently higher δ^{98}Mo value (Fig. 6). This isotopic offset is inconsistent with Mo release by reductive dissolution of metal oxides, which would create much lower δ^{98}Mo values in the pore water. Furthermore, Fe oxides are unlikely to persist in the sulfidic pore fluids of the sediments (Canfield et al., 1993). The fluids in the fluffy surface sediment layers contain mixed δ^{98}Mo values between isotopically heavy Mo from the sulfidic water column (1.8‰) and isotopically light Mo released at ~15 cm depth (1.0‰).

The sinking particles are significantly lighter (0.6 ± 0.1‰) than the sediment. This could suggest several things. One, as mentioned above, is that the release of light Mo during the earliest stages of diagenesis could drive the sediment particles to higher δ^{98}Mo values. Another possibility is that we have not captured sinking particles derived from a very δ^{98}Mo-enriched water column such as we observed during September, 2006. If a 1.0‰ to 1.2‰ offset is to be expected between these heavy water column values and sinking particles, we might predict particles with a δ^{98}Mo of 1.6–1.8‰. These are heavier than the sediment values. A mix of these isotopically enriched particles, together with those captured during August, 2007, could also help explain the sediment values. Unfortunately, we do not know the temporal variability in the δ^{98}Mo of sinking particles.

The dissolved and solid-phase Mo profiles around turbidite deposits at 20 cm depth reveal differences in elemental abundance and isotopic composition which may have persisted over ~50 yrs. There is a dramatic decrease in sediment Mo concentrations, consistent with significant dilution by mountain-sourced debris. These deposits contain ~5 ppm Mo, which is roughly 10 times higher than typical rocks in the catchment area (Table 2), suggesting that these deposits inherited most of their Mo by mixing with lake sediment during deposition. However, its δ^{98}Mo value (0.9–1.0‰) is distinctly lower than the overlying sediments (1.2–1.4‰) which means that it cannot be a result of mixing country rocks with euxinic sediments unless $\delta^{98}Mo_{rocks}$ was extremely low (−1‰), or the underlying sediment was more δ^{98}Mo depleted than what we observe above. Rather, the light δ^{98}Mo in the solid-phase turbidite could appear if light Mo was supplied from an unknown source, for example if sediments from the oxic part of the lake were carried with the turbidite.

5.3. Mo budget for the lake

In order to more fully understand the behavior of molybdenum in the lake, we establish elemental and isotopic mass balances. Despite its small size, this lake (<1 km^2) is quite complicated in terms of its Mo sources and sinks. Fig. 8 shows a compilation of the fluxes that we will now explain.

5.3.1. Elemental mass balance

5.3.1.1. Riverine output. The upper mixolimnion acts as a conveyer moving Mo through the upper lake, a portion of which is captured and removed after diffusing into the chemocline. Surface water enters the lake at several places, but mainly as snow and glacial runoff from mountains at the eastern end. Water exits the western part of the lake and helps drive a local hydroelectric power plant. Water flux is ~3 times higher in the summer months than during winter months, and the seasonal average is $2.0 \pm 0.3 \times 10^9$ L yr^{-1} (data provided by the local hydroelectric power plant). The outlet Mo concentration mirrors the oxic zone at 14 nM and leads to a Mo flux out of the mixolimnion of 29 ± 4 mol yr^{-1}.

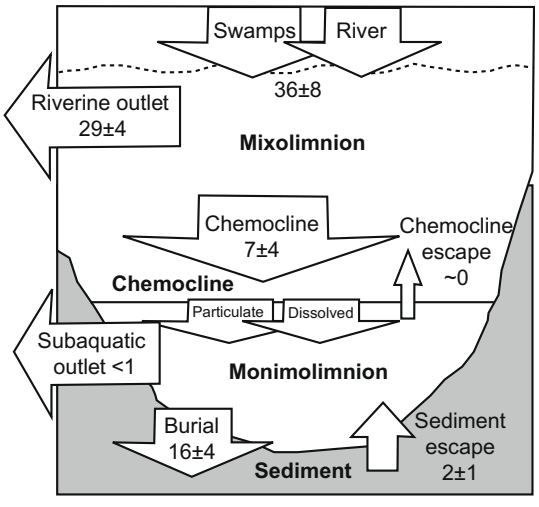

Fig. 8. A generalized box model for Mo sources and sinks in the Lake Cadagno system given in mol yr^{-1} which roughly corresponds to nmol cm^{-2} yr^{-1}. See text for an evaluation of fluxes.

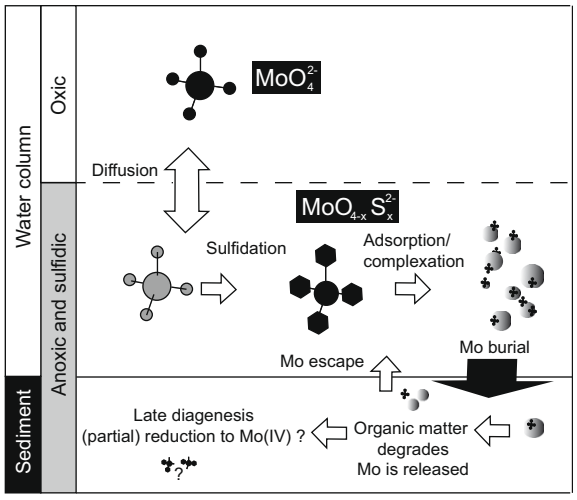

Fig. 9. Schematic overview of the proposed Mo burial pathway from water column to sediments, and Mo release in the sediments. Isotope fractionation occurs during sulfidation of molybdate to particle-reactive thiomolybdate, but a net isotope fractionation will not be expressed in the sediment relative to the input sources ($\delta^{98}Mo_{sediments} = \delta^{98}Mo_{source}$) when Mo is quantitatively removed.

5.3.1.2. Chemocline flux. Dissolved compounds are transported across the chemocline by eddy diffusion. The vertical eddy diffusion coefficient depends on the density stratification of the water and is calculated from the profiles of temperature, conductivity, and turbidity, yielding $K_z = 4{\cdot}10^{-3}$ cm^2 s^{-1} at 7–11 m depth (Electronic annex B). This value is in agreement with dye experiments ($5–10 \times 10^{-3}$ cm^2 s^{-1} (Uhde, 1992), and the value $4.1 \pm 1.3 \times 10^{-3}$ cm^2 s^{-1} obtained from sulfur mass balance (matching rates of sulfate reduction in the lake and the sulfide gradient; Electronic annex B). We use $K_z = 4 \times 10^{-3}$ cm^2 s^{-1} and find net downwards Mo fluxes of 2.2, 9.8 and 8.7 nmol cm^{-2} yr^{-1} across the chemocline for June 2006, September 2006, and August 2007, respectively. This gives a mean value of 7 ± 4 nmol cm^{-2} yr^{-1} (1σ). We have considered that the chemocline was positioned at a shallower depth in June 2006 and thus covered a larger area.

5.3.1.3. Mo sedimentation rate. The net Mo flux to the sediment can be calculated in two ways. First, the radiotracers, ^{210}Pb and ^{137}Cs have been used to calculate a sedimentation rate, s, of 4–6 mm/yr (Birch et al., 1996). In combination with water content and wet density of the sediment, the dry Mo concentrations at the surface are converted to deposition rates, yielding 16 ± 4 nmol Mo cm^{-2} yr^{-1} and 16 ± 3 nmol Mo cm^{-2} yr^{-1} for core J and core 1, respectively. Alternatively, one can use the turbidite deposit as a time marker, because the turbidite was caused by an avalanche in 1951, and then integrate the total Mo deposition to obtain the average Mo deposition rate over 56 yrs. The depth of the turbidite is marked by a sudden drop in water content, β, Loss on Ignition (LOI) and [Mo] at $z = 19.6$ cm depth in core 1.

$$F_{sed} = \int_{0cm}^{turbidite} \rho \cdot (1-\beta) \cdot [Mo]_{sed} dz \quad (1)$$

(ρ = density of wet sediment). This second approach yields an average deposition rate of 20 nmol Mo cm^{-2} yr^{-1} into the sulfidic sediments which is equivalent to 20 mol yr^{-1} when the mean sulfidic lake floor area is equivalent to the area of the chemocline at 11 m depth (Del Don et al., 2001). It appears that the deposition flux of Mo to the sediments of the euxinic zone exceeds the flux of Mo through the chemocline by eddy diffusion, indicating an apparently substantial Mo flux through subaquatic springs.

5.3.1.4. Sediment return flux. The combination of increasing pore water Mo concentrations and decreasing solid-phase Mo (and Mo/Ti) and the consistent isotope behaviors suggests a net flux from the pore water towards the water column. The average mobilization rate from the deep sediment can be derived from linear fits of the sediment Mo/Ti profile in Fig. 6b, and the average sedimentary Ti concentration above 8 cm, $[Ti]_{mean} \sim 2000$ ppm.

$$F_{sed} = -s \cdot \rho \cdot (1-\beta) \frac{\delta(Mo/Ti)}{\delta z} [Ti]_{mean} \quad (2)$$

This leads to a return flux of 3.1 ± 1.2 and 0.7 ± 0.4 nmol cm^{-2} yr^{-1} for core J and core 1, respectively. A much larger return flux is calculated from the pore water profiles using the diffusion coefficient for sulfate (The diffusion coefficient for molybdate is not known, and it is assumed similar to sulfate: $D = 0.572\ 10^{-5}$ cm^2 s^{-1}; Schulz, 2006), and the concentration gradient for Mo obtained by fitting the profiles at 0–8 cm depth (above the sulfide peak) to a 2nd or 3rd order polynomial, $p(z)$, (giving $R^2 > 0.9$), and use $\frac{\delta[Mo]}{\delta z} = p'(z)|_{z=0}$ in the flux equation $F_{pw} = -\Phi D \frac{\delta[Mo]}{\delta z}$, where porosity is determined by $\Phi = \rho{\cdot}\beta$. The calculated fluxes are 15 ± 3 nmol cm^{-2} yr^{-1} and 5 ± 2 nmol cm^{-2} yr^{-1} and comparable to the deposition fluxes ($\sim$16 nmol cm^{-2} yr^{-1}). We suspect, however, that Mo is transported in dissolved phase as humic complexes, with a much lower diffusion coefficient than the free diffusion coefficient. In fact, both of the pore water profiles yields the Mo return flux as derived from the decreasing sedimentary Mo profile if the diffusion coefficient Mo is that of dissolved organic matter, 0.12×10^{-5} cm^2 s^{-1} (Burdige et al., 1999). We, therefore, favor the lower flux estimates based on the solid-phase profiles.

5.3.1.5. Elemental mass balance. A generalized Mo budget for the monimolimnion includes two inaccessible subaquatic components. These are the flux of Mo into the anoxic zone from subaquatic springs (F_{sub}), which deliver the denser bottom water to the lake (Del Don et al., 2001), and any subaquatic flux out of the lake ($F_{sub,out}$). These can be included in an overall mass balance equation (Eq. (3)), with the additional terms: F_{chem} is the flux into the anoxic zone across the chemocline, F_{sed} is the deposition flux to the sediment surface and $F_{sed,loss}$ is the return Mo flux from the sediments to the water column.

$$dMo/dt = F_{chem} + F_{sub} + F_{sed,loss} - F_{sed} - F_{sub,out} \quad (3)$$

In steady state, the net subaquatic Mo source would be F_{sub}–$F_{sub,out} = 7.2 \pm 6.4$ mol/yr ($F_{chem} = 6.9 \pm 4.1$, $F_{sed,loss} = 1.9 \pm 1.2$, $F_{sed} = 16 \pm 3$). The subaquatic Mo

Table 7
Mo fluxes in Lake Cadagno.

		$\delta^{98/95}$Mo (‰)	Element budget flux (nmol cm^{-2} yr^{-1})	Fraction of sediment output
Sediment	Particulate	1.2 ± 0.1	16 ± 4	1
Chemocline	Dissolved	0.9 ± 0.1	6.9 ± 4.1	0.43 ± 0.27
Isotopic constraint		7.2 ± 4.2	0.45 ± 0.28	
Sediment loss	Dissolved	1.0 ± 0.1	1.9 ± 1.2	0.12 ± 0.08
Ground water in	Dissolved	1.55 ± 0.1	7.2 ± 6.4	0.45 ± 0.35
Ground water out	Dissolved	1.8 ± 0.1	<1.2	<0.08

outflow is likely negligible compared to the subaquatic influx. It would carry the Mo concentration of the sulfidic zone, and since its water flux is minor compared to the subaquatic inlet (or the lake would dry out) which carries >20 nM Mo (details in Electronic annex B). Our mass balance indicates a subaquatic Mo source of roughly the same magnitude as the chemocline flux. The model gives a residence time for Mo in the sulfidic zone of 80–130 days using $\tau = M/F_{sed}$ where M is the total Mo inventories (EA-Table A3).

5.3.1.6. Isotope budget. The sediment is significantly enriched in ^{98}Mo compared to the oxic reservoir and this implies an additional heavy source of Mo to the deep lake. We propose that subaquatic springs provide that heavy source. Evidence form Sr isotopes (Electronic annex B) shows that the subaquatic springs are sourced in dolomitic limestone and nearby outcrops reveal a δ^{98}Mo value close to 1.55‰ (Table 2). Therefore, if the dolomite is also the source of the Mo, the surface sediment isotope composition is balanced between the dolomitic subaquatic source, the riverine input, and the return flux of sediment Mo to the water column.

$$\mathrm{Mo}\cdot d/dt(\delta_{sulfidic}) = 0 = F_{\mathrm{chem}}\delta_{\mathrm{chem}} + F_{\mathrm{sub}}\delta_{\mathrm{sub}} + F_{\mathrm{sed,loss}}\delta_{\mathrm{sed,loss}} - F_{\mathrm{sed}}\delta_{\mathrm{sed}} \quad (4)$$

The isotopic budget leads to the same conclusion as the concentration mass balance (Table 7) that the subaquatic springs must accounts for about 7.2 ± 4.2 nmol cm^{-2} yr^{-1} or 45 ± 28% of the Mo burial flux.

In the budget established here, all Mo entering the sulfidic zone is buried and, hence, Mo is quantitatively removed to the sediments. This is justified by considering the large fractionation factors involved in sulfidation reactions (~1.7‰) and the small offset between sediment and any of the sources to the lake (ca. −0.3‰ and +0.3‰ for subaquatic and riverine supply, respectively), which makes it impossible to accommodate a substantial Mo loss from the sulfidic zone.

5.4. Implications

Isotope fractionation during burial into sulfidic sediments has direct implications for interpretation of the paleo-ocean redox conditions for marine sediments. Lake Cadagno compares with marine euxinic systems such as the Black Sea and the Cariaco Basin in terms of Mo burial rate, sedimentation rate, and sediment Mo concentrations at ~100 ppm (Table 8), but displays a ~100 times steeper sulfide gradient (~100 μM/m). This means that the residence time of sulfide and Mo is much shorter in Cadagno compared to the marine sites, and therefore, Mo is not quantitatively converted to tetrathiomolybdate in the water column. Rather, Mo is removed as intermediate oxythiomolybdate species with distinct isotopic compositions. However, although isotope fractionation occurs during molybdenum removal from the sulfidic waters, little or no net fractionation is expressed in the sediments.

We attempt to clarify this picture, by first reviewing the observational record. Sediments of the Cariaco basin

Table 8
Comparison of governing parameters for Mo removal in sulfidic basins.

Basin units	T (°C)	pH	ΣS^{2-} (μM)	Mo_{ox}/Mo_{sulf}[a]	H_2S[b] (μM)	K_Z (cm^2 s^{-1})	τ_{chemo}[c] (yrs)	Mo (ppm)	Δ_{obs}[d] (‰)	Burial rate (nmol Mo cm^{-2} yr^{-1})
Lake Cadagno	4	7.1 [1]/	275	3.5	176[9]	0.004[1]	0.2	110–130[1]	0.0[7]	12–20[1]
Cariaco Basin	9	7.6[2]	40	1.3	14[9]	0.5[4]	20	150–180[6]	0.5[7]	5–11[8]
Black Sea	4	7.8[3]	380	15	83[9]	0.2[5]	10	30–50[7]	0.0[7]	3–6[9]

[a]Mo_{ox}/Mo_{sulf} is the ratio of Mo concentration in oxic surface water and sulfidic bottom water.
[b]Dissociation of sulfide is calculated by equations in Hershey et al. (1988).
[c]The Mo residence time in the chemocline is estimated $\tau = M_{Mo}/F_{chem} = [Mo_{mean}]\cdot h_{chem}/(K_z\ \delta Mo/\delta z|_{z=chem})$ by interpolation of data from Emerson and Huested (1991) and K_z values from other studies.
[d]$\Delta = \delta^{98}Mo_{source} - \delta^{98}Mo_{sediments}$, where the source for marine settings is sea water and the isotope fractionation observed on sinking particles in Lake Cadagno is finally not expressed in the sediments. References: [1] this study; [2] Astor et al. (2005) [3] Black Sea database online: http://sfp1.ims.metu.edu.tr/; [4] Ho et al. (2004); [5] Neretin et al. (2001); [6] (Arnold et al. (2004)); [7] Neubert et al. (2008), Scott et al. (2008); [9] Emerson and Huested (1991).

are found at $\delta^{98}Mo \approx 3/2\ \delta^{97}Mo = 1.78 \pm 0.12‰$ (Arnold et al., 2004), while seawater is at $\delta^{98}Mo = 2.3 \pm 0.1‰$ (Nakagawa et al., 2008; Siebert et al., 2003), leading to a net isotope fractionation in the sediments of, $\Delta^{98}Mo_{SS} = \delta^{98}Mo_{sediments} - \delta^{98}Mo_{sources} = -0.5‰$. Much larger net fractionations of up to $-3.0‰$ are observed in Black Sea sediments deposited in water depths of down to 300 meters and at H_2S levels of 10 μM or less. At > 500 m depths, H_2S concentrations rise to those levels needed for efficient formation of strongly particle-reactive thiomolybdates, and sediments reproduce the $\delta^{98}Mo$ of seawater (Neubert et al., 2008). Neubert et al. (2008) conclude that sulfide levels influence the extent of fractionation by controlling the kinetics of the conversion of molybdate to the various oxythiomolybdate forms. This is completely consistent with our results, where the high sulfide levels in Lake Cadagno favor the more reactive oxythiomolybdate phases and lower overall fractionations as discussed above.

It is important to emphasize the difference between $\Delta^{98}Mo_{SS}$ and isotope fractionation expressed in situ, on sinking particles relative to dissolved Mo in the sulfidic water column, $\Delta^{98}Mo_{PD}$. Fractionation may well occur in the sulfidic system, $\Delta^{98}Mo_{PD} \neq 0$, while no net fractionation is expressed in the sediments, $\Delta^{98}Mo_{SS} = 0$. This is the case in Lake Cadagno.

We qualitatively evaluate the net isotope fractionation, $\Delta^{98}Mo_{SS}$, by calculating the isotopic composition of sinking particles that accumulate the adsorbed species. The sediments should capture the isotope composition of the sinking particles. Molybdate sulfidation progresses towards tetrathiomolybdate as a function of H_2S concentration and time. We assume all species are in isotopic equilibrium at all times whether in solution or particle-bound. Isotope fractionation results only from the (equilibrium) fractionation factors between oxythiomolybdate species in solution ($\Delta_{molybdate-mono} = \Delta_{mono-di} = 1.4‰$, $\Delta_{di-tri} = \Delta_{tri-tetra} = 1.7‰$) and their partitioning between dissolved and particulate phases. Consequently, $\Delta^{98}Mo_{SS}$ becomes a continuous function of $[H_2S]$, time available for reaction, and the particle affinity for each of the oxythiomolybdate species (Fig. 10). For comparison to natural systems, we suggest the time available for reaction is given by the Mo residence time in the chemocline (see footnote of Table 8). We describe the particle affinities of each species by a partition coefficients $K_i = [MoO_{4-i}S_i^{2-}]_{particulate}/[MoO_{4-i}S_i^{2-}]_{dissolved}$, where i is the number of S atoms in the molecule, which is written short as $K = (K_0, K_1, K_2, K_3, K_4)$. Both particles

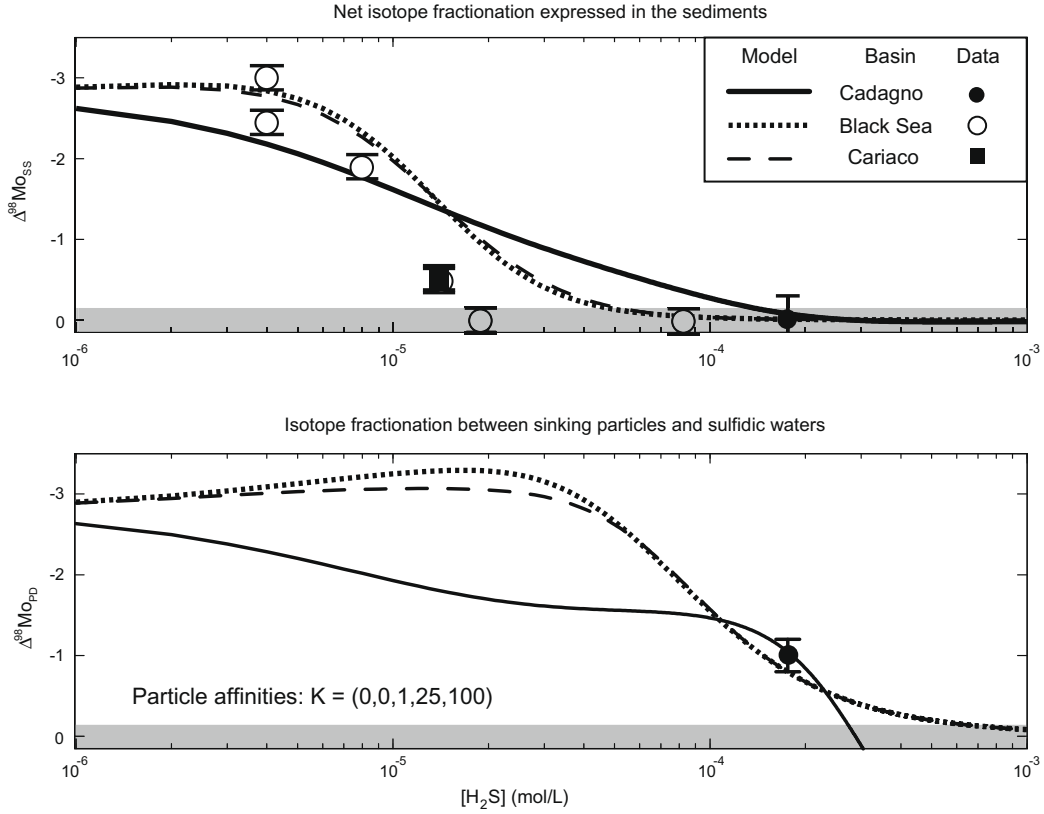

Fig. 10. Model predictions of isotope fractionation expressed in euxinic sediments, $\Delta\delta^{98}Mo_{SS} = \delta^{98}Mo_{sediments} - \delta^{98}Mo_{source}$, as a function of H2S (logarithmic axis). Various lines represent fractionation curves for systems with different time for reaction, Lake Cadagno ($t = 80$ days, solid line), Black Sea ($t = 20$ yrs, dotted line), and Cariaco Basin ($t = 10$ yrs, dashed line). Observed values are shown as error bars using the symbol shown in the legend. In this example, we have chosen the particle affinites for each of the $MoO_{4-x}S_x^{2-}$ species to increase dramatically for tri- and tetrathiomolybdate: $K_0 = K_1 = 0$, $K_2 = 1$, $K_3 = 25$, and $K_4 = 100$. The lower panel shows the predicted isotope fractionation between sinking particles and dissolved Mo, $\Delta\delta^{98}Mo_{PD}$, with the error bar showing observed value from Lake Cadagno. See Appendix C for model details and more examples.

and water contain mixed Mo species allowing for smaller isotopic offset between sinking particles and solution than between any two species. Details on model derivation are found in Electronic annex B.

The predicted net isotope fractionation, $\Delta^{98}Mo_{SS}$, is a strong function of H_2S concentration and depends secondarily on the time available for reaction (Fig. 10). The time dependence is shown in the figure by the various curves, where Lake Cadagno ($t = 80$ days) gives slightly higher fractionation at high H_2S compared to marine settings, Black Sea (20 yrs) and Cariaco Basin (10 yrs) at the same bottom water H_2S concentration. The particle affinities are not constrained by direct measurements; instead we fit these parameters to best match the $\Delta^{98}Mo_{SS}$ data for the three systems, and simultaneously require that the predicted fractionation between sinking particles and dissolved Mo, $\Delta^{98}Mo_{PD}$ (shown in the lower panel) match the observed value $1.0 \pm 0.2‰$ for Lake Cadagno. The model matches data from all three systems reasonably well when the particle affinity is chosen to increase for the more sulfidated species. The best fit is found when the particle affinities for tri- and tetrathiomolybdate are chosen to be much higher than the other oxythiomolybdate species, for example $K = (0, 0, 1, 25,$ and $100)$. This choice of parameters is consistent with the observation that the Mo residence time in the sulfidic zone of Lake Cadagno is comparable to the characteristic time scale of trithiomolybdate formation. The range of possible outcomes for other choices of K is discussed further in Electronic annex C.

Net isotope fractionation, $\Delta^{98}Mo_{SS}$, expressed in sulfidic basins is compared in terms of Mo residence time in the chemocline and H_2S concentrations (Table 8). Highly sulfidic systems such as Lake Cadagno will not express net isotope fractionation, whereas systems such as the shallow Black Sea at or below the 11 μM H_2S threshold of particle-reactive thiomolybdate formation produce high fractionations up to 2–3‰. Systems with short time available for reaction, such as Lake Cadagno, can express net isotope fractionation at 100 μM H_2S, while marine systems have relatively long time for reaction and isotope fractionation remain unexpressed above 50 μM H_2S. For example, the deep Black Sea has ~80 μM H_2S and Mo has a sufficiently long residence time at the chemocline that tetrathiomolybate can form, implying nearly complete Mo drawdown from the water column and no net isotope fractionation expressed in the sediments. The Cariaco Basin has considerable time for reaction, but net isotope fractionation is expressed in the sediments because of low H_2S concentrations close to the 11 μM switch point below which the more particle-reactive tri- and tetrathiomolybdate species effectively never form (Emerson and Huested, 1991; Hershey et al., 1988). Under such conditions, Mo is either removed as $MoO_2S_2^{2-}$ or even MoO_3S^{2-}, or possibly within the sediments where sulfide levels are higher. The model overestimates the observed net isotope fractionation in basins with 10–50 μM H_2S, with higher predicted values for the Cariaco basin (Arnold et al., 2004) and the Black Sea at intermediate depths (Neubert et al., 2008). Possible explanations include (a) temporal [H_2S] variations such that most Mo has been deposited at times of higher sulfide levels, (b) removal occurs in the sediments (at higher H_2S), or (c) the style of removal and its isotopic consequences of Mo adsorption needs be modified.

Our model predicts large fractionations on sinking particles relative to dissolved Mo, $\Delta^{98}Mo_{PD}$ up to 2–3‰, which is expressed in mildly sulfidic sediments of the shallow Black Sea, but not in highly sulfidic sediments. Instead, the model predicts that residual Mo in the sulfidic waters of the deep Black Sea and Cariaco Basin is positively fractionated with $\delta^{98}Mo > \delta^{98}Mo_{sw} = 2.3‰$.

In summary, we have investigated the Mo burial pathway with special attention to the isotopic consequences of Mo burial in sulfidic Lake Cadagno. The lake is used as a modern analogue to show how Mo burial might have progressed in sulfidic Proterozoic oceans. Our analysis suggests that Mo isotopes do fractionate as molybdate is converted to particle-reactive oxythiomolybdate species, and this can be observed on sinking particles which accumulate light Mo, leaving a heavy residual in the dissolved Mo pool of the sulfidic deep waters. However, net isotope fractionation is not expressed in the sediments and marine euxinic sediment deposited in high [H_2S] copy δ^{98}Mo of sea water, consistent with observation in the deep Black Sea. We have established a model for the chemical pathway from source to sediment, and calculate the net fractionation expressed in any sulfidic system as a function of H_2S concentration, time available for reaction, and particle affinities of the oxythiomolybdate species. This model suggests H_2S levels exert primary control on net fractionation in marine basins, where the time available for reaction is long compared to the reaction kinetics of thiomolybdate formation. The model can be tested and refined by laboratory studies of the adsorptive nature of oxythiomolybdate species, e.g. particle affinity, style of particle adsorption, type of material involved, and more field based studies of euxinic systems. Also, we need to understand the Mo removal pathway and diagenetic processes around the 11 μM H_2S threshold where large net isotope fractionations has been observed (Neubert et al., 2008).

6. CONCLUSIONS

We have found that the major burial pathway of Mo in sulfidic Lake Cadagno occurs by particle adsorption in the sulfidic water column. The scavenging process causes a dramatic Mo enrichment in the sediment (~100 ppm) relative to country rocks in the surrounding area (~0.5 ppm) with light Mo preferentially adsorbing to the sinking particles (fractionation of 0.8–1.2‰ between waters and particles). The scavenging particles are most likely organic matter. While isotope fractionation occurs during burial, net isotope fractionation is not expressed, since Mo is quantitatively buried into the sediments from the sulfidic zone. Mo is released during early diagenesis with preferentially light Mo mobilized into the pore fluids (<0.4‰ between sediments and pore fluids). Isotope fractionation associated with the removal process in the water column towards lower δ^{98}Mo values in the sinking particles is most likely to dominate over the positive isotope fractionation resulting from light Mo escape during diagenesis. This results in a

net negative isotope fractionation in the euxinic sediments relative to source waters, simply because the release flux is unlikely to dominate over the Mo deposition rate. The scavenging process at the chemocline removes a range of particle-reactive oxythiomolybdates before the slow reaction kinetics converts all Mo to one species (tetrathiomolybdate). Simple models for the isotope fractionation expressed in euxinic sediments relative to the sources depend on the time available for sulfidation, H_2S concentration, the style of adsorption and the particle affinities for each thiomolybdate species, and negligible net isotope fractionations in highly sulfidic marine systems. Our model results imply that with $[H_2S]$ exceeding about 50 μM, the Mo isotopic composition of ancient seawater will be stored in marine euxinic sediments. Hence, the observed isotope fractionation on sinking particles in Lake Cadagno do not negate the use of the Mo paleo-redox proxy.

ACKNOWLEDGMENTS

We thank Dr. K. Habicht for sharing major ion concentrations (EA-Table C2) and calculated K_z values (EA-Fig. B4), Michael Dalby Kristiansen for sharing CH_4 data, Stephen Romaniello for improvements on double spike data reduction and quality controls and Dr. J. Tossell for sharing theoretically predicted isotope fractionation values. Tom Weber is thanked for fruitful discussions, field trip leader Kirsten Habicht and the SDU/NordCEE crew for arrangements and cooperation with field experiments, Mauro Tonolla and Paola Decristophoris for providing information about the lake and assistance at the field station. Christopher Siebert is thanked for kindly contributing Mo double spike, Jørgen Kystol (GEUS) and Maria Jankowski for laboratory assistance. We thank Derek Vance, Thomas Nägler, and an anonymous reviewer for significant improvements to the manuscript. Financial support was provided by Danish National Research Foundation to Nordic Center for Earth Evolution (NordCEE), The Marine Biological Laboratory's NASA Planetary Biology Internship Program (TWD) and NASA Exobiology Program (NNX07AU15G) and the NSF EAR Instrumentation & Facilities Program (EAR 0520648) to ADA.

APPENDIX A. SUPPLEMENTARY DATA

Supplementary data associated with this article can be found, in the online version, at doi:10.1016/j.gca.2009.09.018.

REFERENCES

Alberic P., Viollier E., Jezequel D., Grosbois C. and Michard G. (2000) Interactions between trace elements and dissolved organic matter in the stagnant anoxic deep layer of a meromictic lake. *Limnol. Oceanogr.* **45**, 1088–1096.

Algeo T. J., Lyons T. W., Blakey R. C. and Over D. J. (2007) Hydrographic conditions of the Devono-Carboniferous North American Seaway inferred from sedimentary Mo-TOC relationships. *Palaeogeogr. Palaeoclimatol. Palaeoecol.* **256**, 204–230.

Anbar A. D., Duan Y., Lyons T. W., Arnold G. L., Kendall B., Creaser R. A., Kaufman A. J., Gordon G. W., Scott C., Garvin J. and Buick R. (2007) A whiff of oxygen before the great oxidation event? *Science* **317**, 1903–1906.

Archer C. and Vance D. (2008) The isotopic signature of the global riverine molybdenum flux and anoxia in the ancient oceans. *Nat. Geosci.* **1**, 597–600.

Arnold G. L., Anbar A. D., Barling J. and Lyons T. W. (2004) Molybdenum isotope evidence for widespread anoxia in mid-Proterozoic oceans. *Science* **304**, 87–90.

Astor Y. M., Scranton M. I., Muller-Karger F., Bohrer R. and Garcia J. (2005) fCO(2) variability at the CARIACO tropical coastal upwelling time series station. *Mar. Chem.* **97**, 245–261.

Barling J. and Anbar A. D. (2004) Molybdenum isotope fractionation during adsorption by manganese oxides. *Earth Planet. Sci. Lett.* **217**, 315–329.

Barling J., Arnold G. L. and Anbar A. D. (2001) Natural mass-dependent variations in the isotopic composition of molybdenum. *Earth Planet. Sci. Lett.* **193**, 447–457.

Birch L., Hanselmann K. W. and Bachofen R. (1996) Heavy metal conservation in Lake Cadagno sediments: Historical records of anthropogenic emissions in a meromictic alpine lake. *Water Res.* **30**, 679–687.

Bostick B. C., Fendorf S. and Helz G. R. (2003) Differential adsorption of molybdate and tetrathiomolybdate on pyrite (FeS_2). *Environ. Sci. Technol.* **37**, 285–291.

Burdige D. J., Berelson W. M., Coale K. H., McManus J. and Johnson K. S. (1999) Fluxes of dissolved organic carbon from California continental margin sediments. *Geochim. Cosmochim. Acta* **63**, 1507–1515.

Canfield D. E., Thamdrup B. and Hansen J. W. (1993) The anaerobic degradation of organic-matter in danish coastal sediments – iron reduction, manganese reduction, and sulfate reduction. *Geochim. Cosmochim. Acta* **57**, 3867–3883.

Canfield D. E. (1998) A new model for Proterozoic ocean chemistry. *Nature* **396**, 450–453.

Cline J. D. (1969) Spectrophotometric determination of hydrogen sulfide in natural waters. *Limnol. Oceanogr.* **14**, 454–458.

Collier R. W. (1985) Molybdenum in the Northeast Pacific-Ocean. *Limnol. Oceanogr.* **30**, 1351–1354.

Crusius J., Calvert S., Pedersen T. and Sage D. (1996) Rhenium and molybdenum enrichments in sediments as indicators of oxic, suboxic and sulfidic conditions of deposition. *Earth Planet. Sci. Lett.* **145**, 65–78.

Del Don C., Hanselmann K. W., Peduzzi R. and Bachofen R. (2001) The meromictic alpine Lake Cadagno: orographical and biogeochemical description. *Aquat. Sci.* **63**, 70–90.

Emerson S. R. and Huested S. S. (1991) Ocean anoxia and the concentrations of molybdenum and vanadium in seawater. *Mar. Chem.* **34**, 177–196.

Erickson B. E. and Helz G. R. (2000) Molybdenum(VI) speciation in sulfidic waters: stability and lability of thiomolybdates. *Geochim. Cosmochim. Acta* **64**, 1149–1158.

Gordon G., Lyons T., Arnold G., Roe J., Sageman B. and Anbar A. (2009) When do black shales tell molybdenum isotope tales? *Geology* **37**, 535–538.

Helz G. R., Miller C. V., Charnock J. M., Mosselmans J. F. W., Pattrick R. A. D., Garner C. D. and Vaughan D. J. (1996) Mechanism of molybdenum removal from the sea and its concentration in black shales: EXAFS evidence. *Geochim. Cosmochim. Acta* **60**, 3631–3642.

Helz G. R., Vorlicek T. P. and Kahn M. D. (2004) Molybdenum scavenging by iron monosulfide. *Environ. Sci. Technol.* **38**, 4263–4268.

Hershey J. P., Plese T. and Millero F. J. (1988) The PK1-$*$ for the dissociation of H_2S in various ionic media. *Geochim. Cosmochim. Acta* **52**, 2047–2051.

Ho T.-Y., Taylor G. T., Astor Y., Varela R., Müller-Karger F. and Scranton M. I. (2004) Vertical and temporal variability of redox

zonation in the water column of the Cariaco Basin: implications for organic carbon oxidation pathways. *Mar. Chem.* **86**, 89–104.

Horwitz E. P., Chiarizia R. and Dietz M. L. (1992) A novel strontium-selective extraction chromatographic resin. *Solvent Extr. Ion Exch.* **10**, 313–336.

Kendall B., Creaser R. A., Gordon G. W. and Anbar A. D. (2009) Re–Os and Mo isotope systematics of black shales from the Middle Proterozoic Velkerri and Wollogorang formations, McArthur Basin, northern Australia. *Geochim. Cosmochim. Acta* **73**, 2534–2558.

Lehmann B., Nagler T. F., Holland H. D., Wille M., Mao J. W., Pan J. Y., Ma D. S. and Dulski P. (2007) Highly metalliferous carbonaceous shale and early cambrian seawater. *Geology* **35**, 403–406.

Morford J. L. and Emerson S. (1999) The geochemistry of redox sensitive trace metals in sediments. *Geochim. Cosmochim. Acta* **63**, 1735–1750.

Nakagawa Y., Firdaus M. L., Norisuye K., Sohrin Y., Irisawa K. and Hirata T. (2008) Precise Mo isotopic analysis on Pacific and Antarctic seawater. In *8th Annual V M Goldschmidt Conference*. Pergamon-Elsevier Science Ltd., Vancouver, Canada.

Neubert N., Nagler T. F. and Bottcher M. E. (2008) Sulfidity controls molybdenum isotope fractionation into euxinic sediments: evidence from the modern Black Sea. *Geology* **36**, 775–778.

Neretin L. N., Volkov I. I., Bottcher M. E. and Grinenko V. A. (2001) A sulfur budget for the Black Sea anoxic zone. *Deep-Sea Res. I Oceanogr. Res. Paper* **48**, 2569–2593.

Pearce C. R., Cohen A. S., Coe A. L. and Burton K. W. (2008) Molybdenum isotope evidence for global ocean anoxia coupled with perturbations to the carbon cycle during the early Jurassic. *Geology* **36**, 231–234.

Peduzzi S., Tonolla M. and Hahn D. (2003) Vertical distribution of sulfate-reducing bacteria in the chemocline of Lake Cadagno, Switzerland, over an annual cycle. *Aquat. Microb. Ecol.* **30**, 295–302.

Putschew A., ScholzBottcher B. M. and Rullkotter J. (1995) Organic geochemistry of sulfur-rich surface sediments of meromictic Lake Cadagno, Swiss Alps. *Geochem. Trans. Sedimentary Sulfur*.

Putschew A., ScholzBottcher B. M. and Rullkotter J. (1996) Early diagenesis of organic matter and related sulphur incorporation in surface sediments of meromictic Lake Cadagno in the Swiss Alps. *Org. Geochem.* **25**, 379–390.

Schulz H.D. and Zabel M. (2006) *Marine Geochemistry*, second ed., Springer Verlag.

Scott C., Lyons T. W., Bekker A., Shen Y., Poulton S. W., Chu X. and Anbar A. D. (2008) Tracing the stepwise oxygenation of the Proterozoic ocean. *Nature* **452**, 456-U5.

Siebert, C., Nagler, T. F. and Kramers, J. D. (2001) Determination of molybdenum isotope fractionation by double-spike multicollector inductively coupled plasma mass spectrometry. *Geochem. Geophys. Geosystems* 2, art. No.-2000GC000124.

Siebert C., Nagler T. F., von Blanckenburg F. and Kramers J. D. (2003) Molybdenum isotope records as a potential new proxy for paleoceanography. *Earth Planet. Sci. Lett.* **211**, 159–171.

Taylor S. R. and McLennon S. M. (1995) The geochemical evolution of the continental crust. *Rev. Geophys.* **33**(2), 241–265.

Tonolla M., Peduzzi S., Hahn D. and Peduzzi R. (2003) Spatio-temporal distribution of phototrophic sulfur bacteria in the chemocline of meromictic Lake Cadagno (Switzerland). *Fems Microbiol. Ecol.* **43**, 89–98.

Tossell J. A. (2005) Calculating the partitioning of the isotopes of Mo between oxidic and sulfidic species in aqueous solution. *Geochim. Cosmochim. Acta* **69**, 2981–2993.

Tucker M. D., Barton L. L. and Thomson B. M. (1998a) Reduction of Cr, Mo, Se and U by *Desulfovibrio desulfuricans* immobilized in polyacrylamide gels. *J. Ind. Microbiol. Biotechnol.* **20**, 13–19.

Tucker M. D., Barton L. L. and Thomson B. M. (1998b) Removal of U and Mo from water by immobilized Desulfovibrio desulfuricans in column reactors. *Biotechnol. Bioeng.* **60**, 88–96.

Uhde M. A. C. (1992) *Mischungsprozesse im Hypolimnion des meromiktischen Lago Cadagno: Eine Untersuchung mit Hilfe natürlicher und künstlicher Tracer*. Diplom Arbeit Albert, Ludwigs-Universität Freiburg.

Viollier E., Jezequel D., Michard G., Pepe M., Sarazin G. and Alberic P. (1995) Geochemical study of a Crater Lake (Pavin Lake, France) – trace-element behavior in the monimolimnion. *Chem. Geol.* **125**, 61–72.

Wasylenki L. E., Rolfe B. A., Weeks C. L., Spiro T. G. and Anbar A. D. (2008) Experimental investigation of the effects of temperature and ionic strength on Mo isotope fractionation during adsorption to manganese oxides. *Geochim. Cosmochim. Acta* **72**, 5997–6005.

Wille M., Nagler T. F., Lehmann B., Schroder S. and Kramers J. D. (2008) Hydrogen sulphide release to surface waters at the Precambrian/cambrian boundary. *Nature* **453**, 767–769.

Winkler L. (1888) *Berichte der Deutschen Chemischen Gesellschaft* **21**, 2843–2855.

Associate editor: George R. Helz